














TECH BRIEFS

NATIONAL AERONAUTICS AND SPACE ADMINISTRATION

-  **Technology Focus**
-  **Electronics/Computers**
-  **Software**
-  **Materials**
-  **Mechanics**
-  **Machinery/Automation**
-  **Manufacturing & Prototyping**
-  **Bio-Medical**
-  **Physical Sciences**
-  **Information Sciences**
-  **Books and Reports**

INTRODUCTION

Tech Briefs are short announcements of innovations originating from research and development activities of the National Aeronautics and Space Administration. They emphasize information considered likely to be transferable across industrial, regional, or disciplinary lines and are issued to encourage commercial application.

Availability of NASA Tech Briefs and TSPs

Requests for individual Tech Briefs or for Technical Support Packages (TSPs) announced herein should be addressed to

National Technology Transfer Center

Telephone No. (800) 678-6882 or via World Wide Web at www2.nttc.edu/leads/

Please reference the control numbers appearing at the end of each Tech Brief. Information on NASA's Innovative Partnerships Program (IPP), its documents, and services is also available at the same facility or on the World Wide Web at <http://ipp.nasa.gov>.

Innovative Partnerships Offices are located at NASA field centers to provide technology-transfer access to industrial users. Inquiries can be made by contacting NASA field centers listed below.

NASA Field Centers and Program Offices

Ames Research Center

Lisa L. Lockyer
(650) 604-1754
lisa.l.lockyer@nasa.gov

Dryden Flight Research Center

Gregory Poteat
(661) 276-3872
greg.poteat@dfrc.nasa.gov

Goddard Space Flight Center

Nona Cheeks
(301) 286-5810
nona.k.cheeks@nasa.gov

Jet Propulsion Laboratory

Ken Wolfenbarger
(818) 354-3821
james.k.wolfenbarger@jpl.nasa.gov

Johnson Space Center

Michele Brekke
(281) 483-4614
michele.a.brekke@nasa.gov

Kennedy Space Center

David R. Makufka
(321) 867-6227
david.r.makufka@nasa.gov

Langley Research Center

Martin Waszak
(757) 864-4052
martin.r.waszak@nasa.gov

Glenn Research Center

Robert Lawrence
(216) 433-2921
robert.f.lawrence@nasa.gov

Marshall Space Flight Center

Vernotto McMillan
(256) 544-2615
vernotto.mcmillan@msfc.nasa.gov

Stennis Space Center

John Bailey
(228) 688-1660
john.w.bailey@nasa.gov

Carl Ray, Program Executive

Small Business Innovation
Research (SBIR) & Small
Business Technology
Transfer (STTR) Programs
(202) 358-4652
carl.g.ray@nasa.gov

Merle McKenzie

Innovative Partnerships
Program Office
(202) 358-2560
merle.mckenzie-1@nasa.gov



TECH BRIEFS

NATIONAL AERONAUTICS AND SPACE ADMINISTRATION



5 Technology Focus: Sensors

- 5 Protein Sensors Based on Optical Ring Resonators
- 6 Phase Sensor for Aligning a Segmented Telescope Mirror
- 6 Control Software for Advanced Video Guidance Sensor
- 6 Generating Control Commands From Gestures Sensed by EMG



9 Electronics/Computers

- 9 Multiple-Flat-Panel System Displays Multidimensional Data
- 10 3D X-Ray Luggage-Screening System
- 11 Probe Station and Near-Field Scanner for Testing Antennas
- 11 Photodetector Arrays for Multicolor Visible/Infrared Imaging
- 12 Semiconductor Bolometers Give Background-Limited Performance
- 13 Multichannel X-Band Dielectric-Resonator Oscillator
- 14 Automatic Alignment of Displacement-Measuring Interferometer



15 Software

- 15 Earth Observing System Data Gateway
- 15 Power User Interface
- 15 Mercury Shopping Cart Interface
- 15 Cassini Archive Tracking System
- 16 Architecture Adaptive Computing Environment
- 16 Computing Fault Displacements From Surface Deformations



17 Materials

- 17 Oxygen-Permeable, Hydrophobic Membranes of Silanized α -Al₂O₃
- 17 SiC Composite Turbine Vanes



19 Mechanics

- 19 Retaining Device for the Interior Structure of a Spacecraft Payload
- 19 Tool for Torquing Circular Electrical-Connector Collars



21 Machinery/Automation

- 21 System for Continuous Deaeration of Hydraulic Oil
- 22 Solar-Powered Cooler and Heater for an Automobile Interior



23 Manufacturing & Prototyping

- 23 Improved Oxygen-Beam Texturing of Glucose-Monitoring Optics
- 23 Tool for Two Types of Friction Stir Welding



25 Bio-Medical

- 25 Stationary Apparatus Would Apply Forces of Walking to Feet
- 25 Instrument Would Detect and Collect Biological Aerosols



27 Physical Sciences

- 27 Boundary Condition for Modeling Semiconductor Nanostructures
- 28 Miniature Distillation Column for Producing LOX From Air
- 29 Even Illumination From Fiber-Optic-Coupled Laser Diodes
- 30 Optically Driven Deformable Mirrors



31 Information Sciences

- 31 Algorithm for Automated Detection of Edges of Clouds
- 31 Exploiting Quantum Resonance to Solve Combinatorial Problems
- 31 Hybrid Terrain Database



33 Books & Reports

- 33 On Release of Microbe-Laden Particles From Mars Landers
- 33 A Concept for Run-Time Support of the Chapel Language
- 33 Thermoelectric Inhomogeneities in (Ag_{1-y}SbTe₂)_x(PbTe)_{1-x}
- 33 Spacecraft Escape Capsule

This document was prepared under the sponsorship of the National Aeronautics and Space Administration. Neither the United States Government nor any person acting on behalf of the United States Government assumes any liability resulting from the use of the information contained in this document, or warrants that such use will be free from privately owned rights.



Protein Sensors Based on Optical Ring Resonators

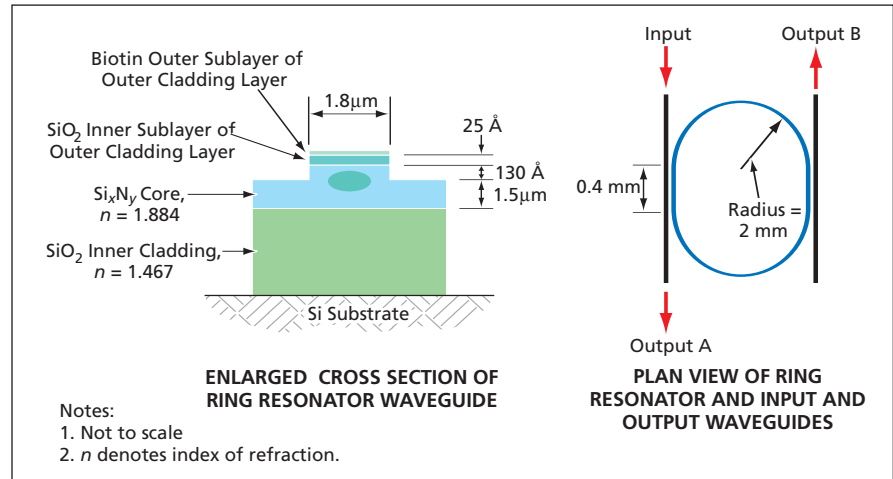
Progress has been achieved in the continuing development of optical chemical sensors.

NASA's Jet Propulsion Laboratory, Pasadena, California

Prototype transducers based on integrated optical ring resonators have been demonstrated to be useful for detecting the protein avidin in extremely dilute solutions. In an experiment, one of the transducers proved to be capable of indicating the presence of avidin at a concentration of as little as 300 pM in a buffer solution — a detection sensitivity comparable to that achievable by previously reported protein-detection techniques. These transducers are serving as models for the further development of integrated-optics sensors for detecting small quantities of other proteins and proteinlike substances.

The basic principle of these transducers was described in "Chemical Sensors Based on Optical Ring Resonators" (NPO-40601), *NASA Tech Briefs*, Vol. 29, No. 10 (October 2005), page 32. The differences between the present transducers and the ones described in the cited prior article lie in details of implementation of the basic principle. As before, the resonator in a transducer of the present type is a closed-circuit dielectric optical waveguide. The outermost layer of this waveguide, analogous to the optical cladding layer on an optical fiber, consists of a layer comprising sublayers having indices of refraction lower than that of the waveguide core. The outermost sublayer absorbs the chemical of interest (in this case, avidin). The index of refraction of the outermost sublayer changes with the concentration of absorbed avidin. The resonator is designed to operate with relatively strong evanescent-wave coupling between the outer sublayer and the electromagnetic field propagating along the waveguide core. By virtue of this coupling, the chemically induced change in the index of refraction of the outermost sublayer causes a measurable change in the spectrum of the resonator output.

The figure depicts one of the prototype transducers, wherein the ring resonator is a dielectric optical waveguide laid out along a closed path resembling a racetrack. The waveguide includes a



A Biotin-Clad Optical Ring Resonator acts as an avidin sensor in that the resonance spectrum becomes shifted in wavelength when the biotin absorbs avidin.

core of Si_3N_4 formed on an inner cladding layer of SiO_2 on a substrate of Si. The outer cladding layer comprises an inner sublayer of SiO_2 and an outer sublayer of biotin. (The SiO_2 sublayer is needed for binding the biotin to the Si_3N_4 core.) The selectivity of the sensor depends on the use of biotin, which binds specifically to avidin, immobilizing avidin on the outer surface and thereby changing the index of refraction. The portion of the cross section occupied by the propagating electromagnetic mode is confined laterally by the rib portion of the core and is shown in the figure as an oval. In addition to the ring resonator, there are straight input and output waveguides separated from the straight segments of the ring resonator by an evanescent-wave-coupling gap of 1.6 μm .

In operation, the transducer is mounted in a flow cell on a copper chuck. The temperature of the chuck (and, thus, of the transducer) is monitored by use of a thermistor and controlled by use of a thermoelectric cooler. A solution containing avidin is pumped through the flow cell. Through the straight input waveguide, the resonator is illuminated at a wavelength of 633 nm by a He-Ne laser. The length of the closed optical path of the resonator ring varies with the temperature, and the

temperature is adjusted to keep the path length an integer multiple of a wavelength: that is, the temperature is adjusted to maintain operation at one of the resonances. As the biotin coating absorbs avidin, the resulting change in the index of refraction manifests itself as a change in the resonance wavelength and, hence, in the temperature needed to maintain the chosen resonance. Hence, further, the change in the controlled temperature can be taken as an indication of the amount of dissolved avidin to which the transducer has been exposed.

This work was done by Ying Lin and Alexander Ksendzov of Caltech for NASA's Jet Propulsion Laboratory. Further information is contained in a TSP (see page 1).

In accordance with Public Law 96-517, the contractor has elected to retain title to this invention. Inquiries concerning rights for its commercial use should be addressed to:

Innovative Technology Assets Management
JPL

Mail Stop 202-233
4800 Oak Grove Drive
Pasadena, CA 91109-8099
(818) 354-2240

E-mail: iaoffice@jpl.nasa.gov
Refer to NPO-41585, volume and number of this NASA Tech Briefs issue, and the page number.

Phase Sensor for Aligning a Segmented Telescope Mirror

Alignment can be maintained even in the presence of atmospheric turbulence.

Marshall Space Flight Center, Alabama

A phase sensor has been developed for use in aligning a segmented telescope mirror to within a fraction of a wavelength in piston. (As used here, "piston" signifies displacement of a mirror segment along the optical axis of the telescope.) Such precise alignment is necessary in order to realize the full benefit of the large aperture achievable through segmentation.

This phase sensor is achromatic. It is based on two-wavelength shearing interferometry, and can be modified to utilize an extended or broad-band (e.g., white) light source. The sensor optics include a ruled diffraction grating and an imaging lens.

The sensor can measure the piston shift between segments as well as aberrations of the segments. It can measure

the surface error of an individual segment, making it possible to compensate for the error with optimal amount(s) of piston and/or tilt. The precise capture range of the sensor depends partly on the telescope design; the largest relative piston shifts measurable by use of this sensor are of the order of 100 μm . The accuracy of the sensor also depends partly on the telescope design; in general, the accuracy is sufficient to enable alignment to within approximately half a wavelength. The interferometric image is digitized and processed by a simple algorithm in real time, and the output of the algorithm can be used to maintain alignment in real time, even in the presence of atmospheric turbulence.

The sensor is robust. Through calibration, it can be made insensitive to (and, hence, tolerant of) misalignments and aberrations of its own optics, most aberrations of the telescope as a whole (in contradistinction to aberrations of individual segments), and most aberrations introduced by atmospheric turbulence.

This work was done by H. Philip Stahl of Marshall Space Flight Center and Chanda Bartlett Walker of Pace & Waite, Inc. Further information is contained in a TSP (see page 1).

This invention is owned by NASA, and a patent application has been filed. For further information, contact Sammy Nabors, MSFC Commercialization Assistance Lead, at sammy.a.nabors@nasa.gov. Refer to MFS-31852-1.

Control Software for Advanced Video Guidance Sensor

Marshall Space Flight Center, Alabama

Embedded software has been developed specifically for controlling an Advanced Video Guidance Sensor (AVGS). [As described in several previous *NASA Tech Briefs* articles, a Video Guidance Sensor is an optoelectronic system that provides guidance for automated docking of two vehicles (spacecraft in the original intended application). Such a system includes pulsed laser diodes and a video camera, the output of which is digitized. From the positions of digitized target images and known geometric relationships, the relative position and orientation of the vehicles are computed.] The present software consists of two sub-

programs running in two processors that are parts of the AVGS. The subprogram in the first processor receives commands from an external source, checks the commands for correctness, performs commanded non-image-data-processing control functions, and sends image-data-processing parts of commands to the second processor. The subprogram in the second processor processes image data as commanded. Upon power-up, the software performs basic tests of functionality, then effects a transition to a standby mode. When a command is received, the software goes into one of several operational modes (e.g. acquisition

or tracking). The software then returns, to the external source, the data appropriate to the command.

This program was written by Richard T. Howard, Michael L. Book, and Thomas C. Bryan of Marshall Space Flight Center. Further information is contained in a TSP (see page 1).

This invention has been patented by NASA (U.S. Patent No. 6,888,476). Inquiries concerning nonexclusive or exclusive license for its commercial development should be addressed to Sammy Nabors, MSFC Commercialization Assistance Lead, at sammy.a.nabors@nasa.gov. Refer to MFS-31865-1.

Generating Control Commands From Gestures Sensed by EMG

Electrical signals from muscles involved in gestures are recognized.

Ames Research Center, Moffett Field, California

An effort is under way to develop noninvasive neuro-electric interfaces through which human operators could control systems as diverse as simple mechanical devices, computers, aircraft, and even space-

craft. The basic idea is to use electrodes on the surface of the skin to acquire electromyographic (EMG) signals associated with gestures, digitize and process the EMG signals to recognize the gestures,

and generate digital commands to perform the actions signified by the gestures.

In an experimental prototype of such an interface, the EMG signals associated with hand gestures are acquired by use

of several pairs of electrodes mounted in sleeves on a subject's forearm (see figure). The EMG signals are sampled and digitized. The resulting time-series data are fed as input to pattern-recognition software that has been trained to distinguish gestures from a given gesture set. The software implements, among other things, hidden Markov models, which are used to recognize the gestures as they are being performed in real time.

Thus far, two experiments have been performed on the prototype interface to demonstrate feasibility: an experiment in synthesizing the output of a joystick and an experiment in synthesizing the output of a computer or typewriter keyboard. In the joystick experiment, the EMG signals were processed into joystick commands for a realistic flight simulator for an airplane. The acting pilot reached out into the air, grabbed an imaginary joystick, and pretended to manipulate the joystick to achieve left and right banks and up and down pitches of the simulated airplane. In the keyboard experiment, the subject pretended to type on a numerical keypad, and the EMG signals were processed into keystrokes.

The results of the experiments demonstrate the basic feasibility of this method while indicating the need for further research to reduce the incidence of errors (including confusion among gestures). Topics that must be addressed include the numbers and arrangements of electrodes needed to acquire sufficient data; refinements in the acquisi-



Electrodes on a Subject's Forearm were used to acquire EMG signals in experiments on synthesizing joystick attitude controls for simulated airplane flight and synthesizing typing on a numerical keypad.

tion, filtering, and digitization of EMG signals; and methods of training the pattern-recognition software.

The joystick and keyboard simulations were chosen for the initial experiments because they are familiar to many computer users. It is anticipated that, ultimately, interfaces would utilize EMG signals associated with movements more nearly natural than those associated with joysticks or keyboards. Future versions of the pattern-recognition software are planned to be capable of adapting to the preferences and day-to-day variations in EMG outputs of individual users; this capability for adaptation would also make it possible to

select gestures that, to a given user, feel the most nearly natural for generating control signals for a given task (provided that there are enough properly positioned electrodes to acquire the EMG signals from the muscles involved in the gestures).

This work was done by Kevin R. Wheeler and Charles Jorgensen of Ames Research Center. Further information is contained in a TSP (see page 1).

This invention has been patented by NASA (U.S. Patent No. 6,720,984). Inquiries concerning rights for the commercial use of this invention should be addressed to the Ames Technology Partnerships Division at (650) 604-2954. Refer to ARC-14494-1.



Multiple-Flat-Panel System Displays Multidimensional Data

Related images are displayed simultaneously to facilitate perception of trends in data.

Ames Research Center, Moffett Field, California

The NASA Ames hyperwall is a display system designed to facilitate the visualization of sets of multivariate and multidimensional data like those generated in complex engineering and scientific computations. The hyperwall includes a 77 matrix of computer-driven flat-panel video display units, each presenting an image of 1,280x1,024 pixels. The term “hyperwall” reflects the fact that this system is a more capable successor to prior computer-driven multiple-flat-panel display systems known by names that include the generic term “powerwall” and the trade names “PowerWall” and “Powerwall.”

Each of the 49 flat-panel displays is driven by a rack-mounted, dual-central-processing-unit, workstation-class personal computer equipped with a high-performance graphical-display circuit card and with a hard-disk drive having a storage capacity of 100 GB. Each such computer is a slave node in a master/slave computing/data-communication system (see Figure 1). The computer that acts as the master node is similar to the slave-node computers, except that it runs the master portion of the system software and is equipped with a keyboard and mouse for control by a human operator. The system utilizes commercially available master/slave software along with custom software that enables the human controller to interact simultaneously with any number of selected slave nodes.

In a powerwall, a single rendering task is spread across multiple processors and then the multiple outputs are tiled into one seamless superdisplay. It must be noted that the hyperwall concept subsumes the powerwall concept in that a single scene could be rendered as a mosaic image on the hyperwall. However, the hyperwall offers a wider set of capabilities to serve a different purpose: The hyperwall concept is one of (1) simultaneously displaying multiple different but related images, and (2) providing means for composing and controlling such sets of images. In place of elaborate software or hardware crossbar switches, the hy-

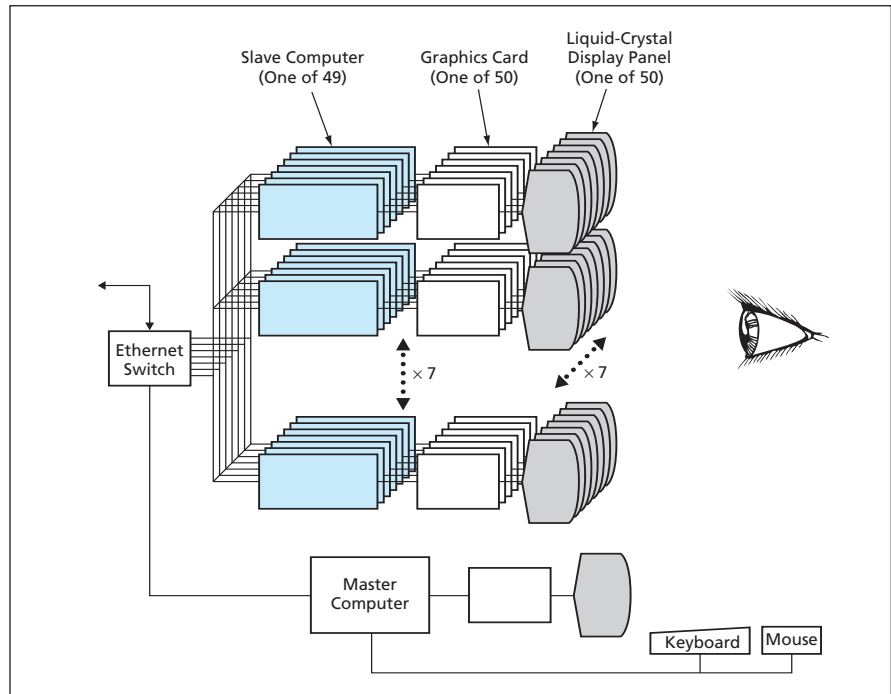


Figure 1. Master and Slave Nodes Communicate via a high-speed local-area network.



Figure 2. Each of 16 Images displayed on a hyperwall represents results of a computational simulation of airflow about an aerospacecraft (specifically, a proposed reusable launch vehicle) at one of 16 different combinations of Mach numbers and angles of attack.

perwall concept substitutes reliance on the human visual system for integration, synthesis, and discrimination of patterns in complex and high-dimensional data spaces represented by the multiple displayed images.

The variety of multidimensional data sets that can be displayed on the hyperwall is practically unlimited. For example, Figure 2 shows a hyperwall display of surface pressures and streamlines from a computational simulation of airflow

about an aerospacecraft at various Mach numbers and angles of attack. In this display, Mach numbers increase from left to right and angles of attack increase from bottom to top. That is, all images in the same column represent simulations at the same Mach number, while all images in the same row represent simulations at the same angle of attack. The same viewing transformations and the same mapping from surface pressure to colors were used in generating all the images.

This work was done by Daniel Gundo and Creon Levit of Ames Research Center; Christopher Henze, Timothy Sandstrom, David Ellsworth, and Bryan Green of Advanced Management Technology, Inc.; and Arthur Joly of Computer Science Corporation. Further information is contained in a TSP (see page 1).

Inquiries concerning rights for the commercial use of this invention should be addressed to the Ames Technology Partnerships Division at (650) 604-2954. Refer to ARC-15037-1.

3D X-Ray Luggage-Screening System

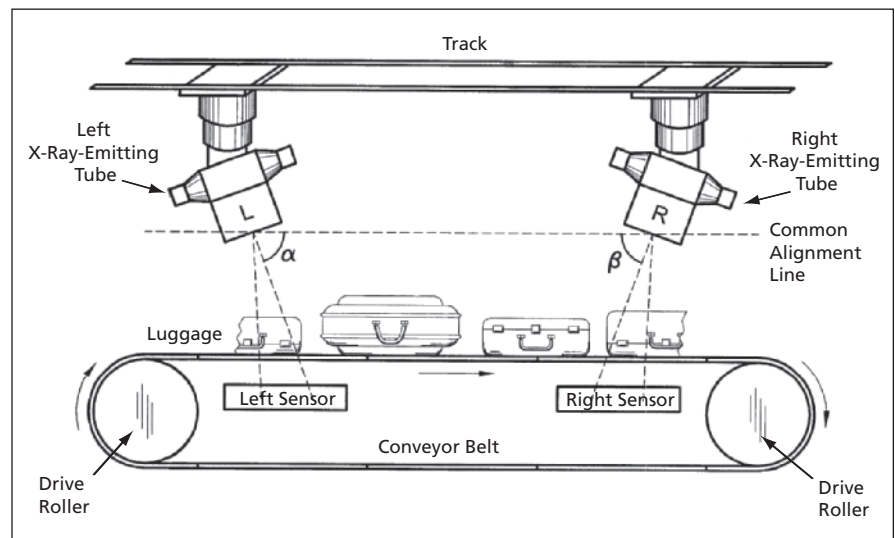
3D displays would help inspectors distinguish among objects at different depths.

Marshall Space Flight Center, Alabama

A three-dimensional (3D) x-ray luggage-screening system has been proposed to reduce the fatigue experienced by human inspectors and increase their ability to detect weapons and other contraband. The system and variants thereof could supplant thousands of x-ray scanners now in use at hundreds of airports in the United States and other countries. The device would be applicable to any security checkpoint application where current two-dimensional scanners are in use.

A conventional x-ray luggage scanner generates a single two-dimensional (2D) image that conveys no depth information. Therefore, a human inspector must scrutinize the image in an effort to understand ambiguous-appearing objects as they pass by at high speed on a conveyor belt. Such a high level of concentration can induce fatigue, causing the inspector to reduce concentration and vigilance. In addition, because of the lack of depth information, contraband objects could be made more difficult to detect by positioning them near other objects so as to create x-ray images that confuse inspectors.

The proposed system would make it unnecessary for a human inspector to interpret 2D images, which show objects at different depths as superimposed. Instead, the system would take advantage of the natural human ability to infer 3D information from stereographic or stereoscopic images. The inspector would be able to perceive two objects at different depths, in a more nearly natural manner, as distinct 3D objects lying at different depths. Hence, the inspector could recognize objects with greater accuracy and less effort.



Images From the Left- and Right-Eye X-Ray Sensors are captured at different locations and stored along with conveyor position data allowing the appropriate left- and right-eye images to be viewed by the human operator on a commercially available stereo display screen.

The major components of the proposed system would be similar to those of x-ray luggage scanners now in use. As in a conventional x-ray scanner, there would be an x-ray source. Unlike in a conventional scanner, there would be two x-ray image sensors, denoted the left and right sensors, located at positions along the conveyor that are upstream and downstream, respectively (see figure). X-ray illumination may be provided by a single source or by two sources. The position of the conveyor would be detected to provide a means of matching the appropriate left- and right-eye images of an item under inspection.

The appropriate right- and left-eye images of an item would be displayed simultaneously to the right and left eyes, respectively, of the human inspector, using

commercially available stereo display screens. The human operator could adjust viewing parameters for maximum viewing comfort. The stereographic images thus generated would differ from true stereoscopic images by small distortions that are characteristic of radiographic images in general, but these distortions would not diminish the value of the images for identifying distinct objects at different depths.

This work was done by Kenneth Fernandez of Marshall Space Flight Center. Further information is contained in a TSP (see page 1).

This invention has been patented by NASA (U.S. Patent No. 6,763,083 B2). Inquiries concerning nonexclusive or exclusive license for its commercial development should be addressed to Sammy Nabors, MSFC Commercialization Assistance Lead, at sammy.a.nabors@nasa.gov. Refer to MFS-31783.

Probe Station and Near-Field Scanner for Testing Antennas

Multiple antennas on the same substrate can be evaluated quickly and inexpensively.

John H. Glenn Research Center, Cleveland, Ohio

A facility that includes a probe station and a scanning open-ended waveguide probe for measuring near electromagnetic fields (see figure) has been added to Glen Research Center's suite of antenna-testing facilities, at a small fraction of the cost of the other facilities. This facility is designed specifically for nondestructive characterization of the radiation patterns of miniaturized microwave antennas fabricated on semiconductor and dielectric wafer substrates, including active antennas that are difficult to test in traditional antenna-testing ranges because of fragility, smallness, or severity of DC-bias or test-fixturing requirements. By virtue of the simple fact that a greater fraction of radiated power can be captured in a near-field measurement than in a conventional far-field measurement, this near-field facility is convenient for testing miniaturized antennas with low gains.

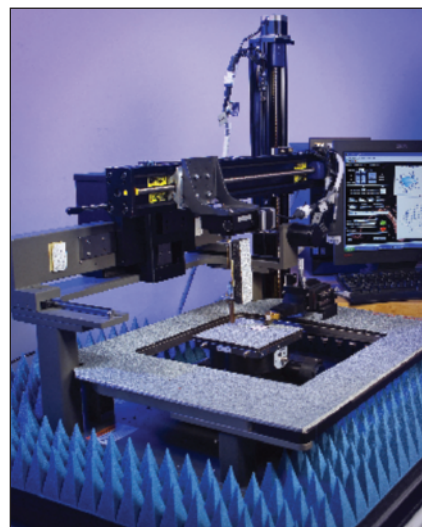
This facility makes it possible to test a complete set or any subset of a multiplicity of antennas on the same substrate in one session. The multiple antennas can all be of the same design or different designs. Unlike in prior antenna-testing facilities, there is no need for wafer-level dicing or packaging to isolate individual antennas from a multiple-antenna substrate before testing, and no need for special test fixtures. Hence, alternative prototype antenna designs can be evaluated in rapid succession to converge on an optimum design in less time (and, hence, at less

cost) than in prior antenna-testing facilities.

In this facility, radio-frequency (RF) signals and DC bias voltages and currents are supplied to an antenna under test (AUT) through RF and DC probes, respectively, that are parts of the probe station. The equipment in this facility includes a commercially available RF probe station, a coplanar-waveguide ground-signal-ground microwave probe that makes contact with the AUT, the aforementioned scanning open-ended waveguide probe, an automatic network analyzer (more specifically, a vector network analyzer)/microwave receiver, and a computer.

The mechanisms for scanning the open-ended waveguide probe are a three-axis slide mechanism and a rotation mechanism that, under computer control, positions this probe for acquisition of data at prescribed grid points on a plane very close to the AUT. This near-field scanning scheme enables capture of a maximum amount of energy radiated by one or multiple small antennas while they are DC-biased, without need for any special fixture.

The system is controlled by user-friendly operational, data-acquisition, and data-analysis software. The dimensions of the near-field scan area and the distance between grid points are specified by the user via the computer keyboard as inputs to a software-generated control panel. After each scan, the data-analysis software processes the measurement data and displays the far-field radiation pattern of the AUT,



The Open-Ended Waveguide Probe Is Scanned in a plane slightly above the AUT and is operated in conjunction with an RF contact probe and the vector network analyzer to gather data on the near radiation field.

computed from the near-field measurements.

This work was done by Afroz Zaman, Richard Q. Lee, William G. Darby, Philip J. Barr, and Félix A. Miranda of **Glenn Research Center**; and Kevin Lambert of **Analex Corp.** Further information is contained in a TSP (see page 1).

Inquiries concerning rights for the commercial use of this invention should be addressed to NASA Glenn Research Center, Innovative Partnerships Office, Attn: Steve Fedor, Mail Stop 4-8, 21000 Brookpark Road, Cleveland, Ohio 44135. Refer to LEW-17877-1.

Photodetector Arrays for Multicolor Visible/Infrared Imaging

Separate optical trains would not be needed for different wavelength bands.

NASA's Jet Propulsion Laboratory, Pasadena, California

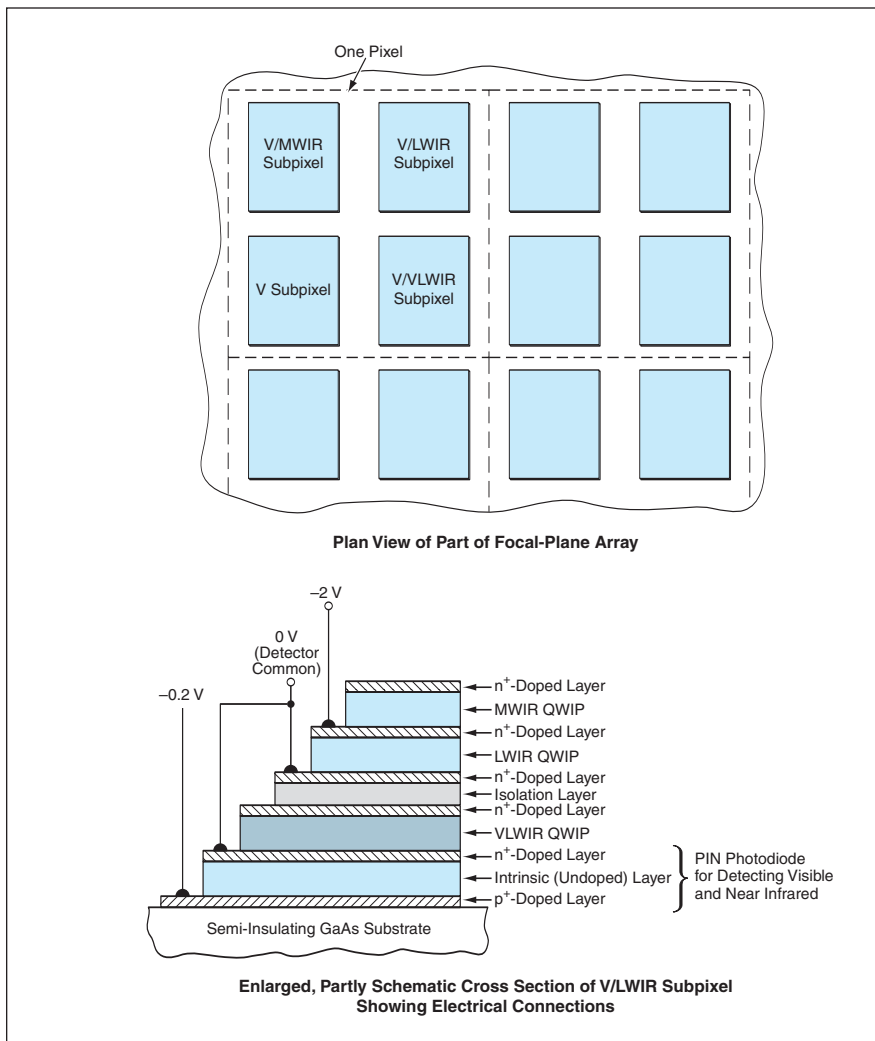
Monolithic focal-plane arrays of photodetectors capable of imaging the same scenes simultaneously in multiple wavelength bands in the visible and infrared spectral regions have been proposed. In prior visible/infrared imaging systems, it has been standard practice to use separate optical trains to form images in visible and infrared wavelength bands on separate visible- and infrared-photodetector arrays. Be-

cause the proposal would enable the detection of images in multiple wavelength bands on the same focal plane, the proposal would make it unnecessary to use multiple optical trains. Hence, multispectral imaging systems could be made more compact and the difficulties of aligning multiple optical trains would be eliminated.

Each pixel in an array according to the proposal would contain stacks of sev-

eral photodetectors. The proposal is a logical extension of prior concepts of arrays of stacked photodetectors for imaging in two or three wavelength bands. For example, such an array was described in "Three-Color Focal-Plane Array of Infrared QWIPs" (NPO-20683), *NASA Tech Briefs*, Vol. 24, No. 5 (May 2000), page 26a.

In one proposed design, (see figure), each pixel would be divided into four



Each Pixel of a Four-Color Focal-Plane Array would be divided into four subpixels containing stacked photodetectors for four wavelength bands. The pixels would be identical except for the electrical connections for activating the detectors for different wavelength-band combinations.

subpixels, one being dedicated to a visible-and-near-infrared (V) band, one to a combination of the V band and a very-long-wavelength infrared (VLWIR) band, one to a combination of the V band and a long-wavelength infrared (LWIR) band, and one to a combination of the V band and a medium-wavelength infrared (MWIR) band. For this purpose, each subpixel would include a GaAs-based positive/intrinsic/negative (PIN) photodiode for detection in the V band stacked with three quantum-well infrared photodetectors (QWIPs), each optimized for one of the aforementioned infrared bands. The stacks of photodetectors in all the subpixels would be identical except for the electrical connections, which would be configured to activate the various wavelength-band combinations.

This work was done by Sarath Gunapala, Sumith Bandara, John Liu, and David Ting of Caltech for NASA's Jet Propulsion Laboratory. Further information is contained in a TSP (see page 1).

In accordance with Public Law 96-517, the contractor has elected to retain title to this invention. Inquiries concerning rights for its commercial use should be addressed to:

*Innovative Technology Assets Management
JPL*

*Mail Stop 202-233
4800 Oak Grove Drive
Pasadena, CA 91109-8099
(818) 354-2240*

E-mail: iaoffice@jpl.nasa.gov

Refer to NPO-30541, volume and number of this NASA Tech Briefs issue, and the page number.

Semiconductor Bolometers Give Background-Limited Performance

These devices can be fabricated inexpensively by use of established silicon-processing techniques.

Ames Research Center, Moffett Field, California

Semiconductor bolometers that are capable of detecting electromagnetic radiation over most or all of the infrared spectrum and that give background-limited performance at operating temperatures from 20 to 300 K have been invented. The term "background-limited performance" as applied to a bolometer, thermopile, or other infrared detector signifies that the ability to detect infrared signals that originate outside the detector is limited primarily by thermal noise attributable to the background radiation generated external to the bolometer. The signal-to-noise ratios and detectivities of the bolometers and

thermopiles available prior to this invention have been lower than those needed for background-limited performance by factors of about 100 and 10, respectively.

Like other electrically resistive bolometers, a device according to the invention exhibits an increase in electrical resistance when heated by infrared radiation. Depending on whether the device is operated under the customary constant-current or constant-voltage bias, the increase in electrical resistance can be measured in terms of an increase in voltage across the device or a decrease in current through the device, respectively.

In the case of a semiconductor bolometer, it is necessary to filter out visible and shorter-wavelength light that could induce photoconductivity and thereby counteract all or part of the desired infrared-induced increase in resistance.

The basic semiconductor material of a bolometer according to the invention is preferably silicon doped with one or more of a number of elements, each of which confers a different variable temperature coefficient of resistance. Suitable dopants include In, Ga, S, Se, Te, B, Al, As, P, and Sb. The concentration of dopant preferably lies in the range between 0.1 and 1,000 parts per billion.

The dopant and its concentration are chosen to optimize the performance of the bolometer, taking account of the bolometer operating temperature, the temperature of the source of infrared radiation to be detected, and other relevant environmental factors.

An important practical advantage of the use of silicon, in contradistinction to other semiconductors, is that the art of fabrication of electronic devices from sili-

con is mature, enabling mass production at low cost per device. An additional advantage accrues when indium is used as the dopant: Indium can be incorporated into silicon over a wide range of concentrations with little consequent change in the basic structure of the silicon matrix. Hence, with impunity, the concentration of indium dopant can be set at almost any desired value in an effort to obtain the desired electrical impedance.

This work was done by John Goebel and Robert McMurray of Ames Research Center. Further information is contained in a TSP (see page 1).

This invention has been patented by NASA (U.S. Patent No. 6,838,669). Inquiries concerning rights for the commercial use of this invention should be addressed to the Ames Technology Partnerships Division at (650) 604-2954. Refer to ARC-14577.

Multichannel X-Band Dielectric-Resonator Oscillator

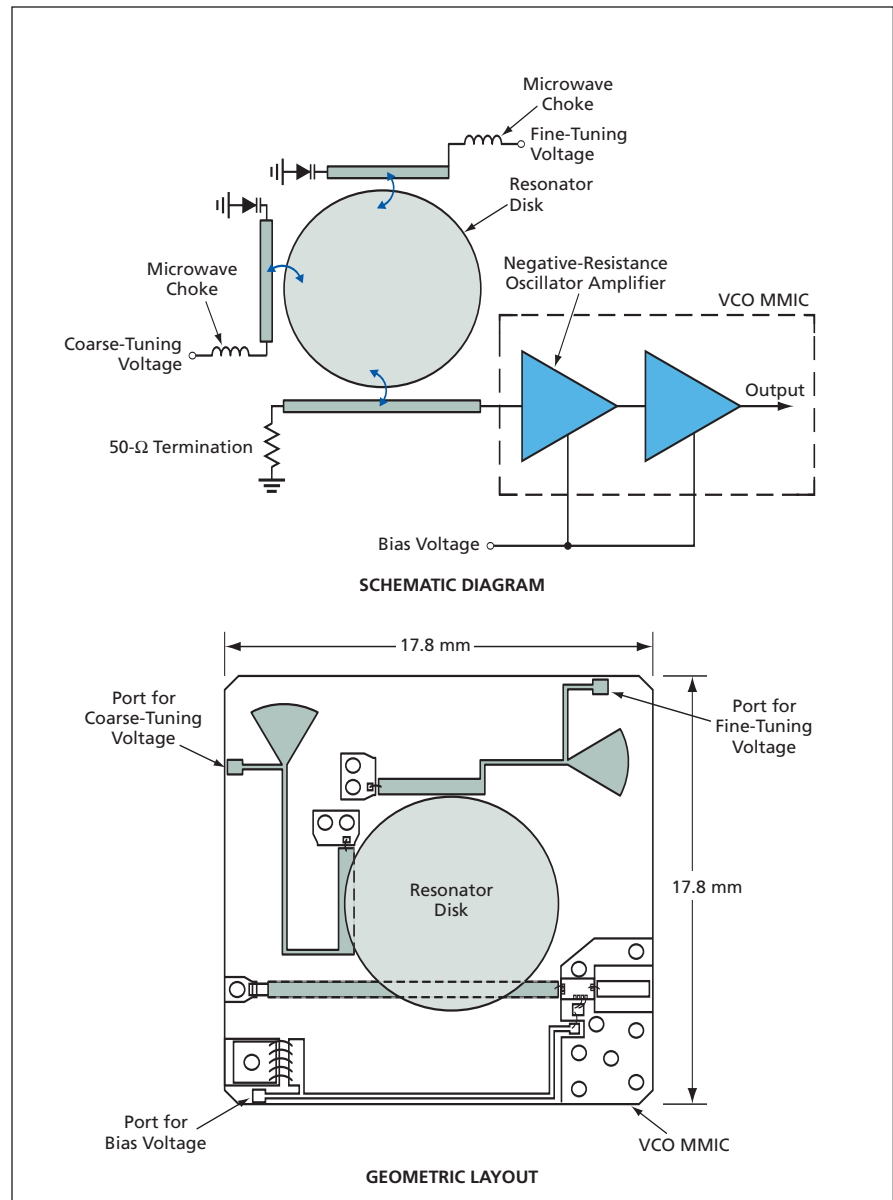
Unlike other DROs, this one is electrically tunable.

NASA's Jet Propulsion Laboratory, Pasadena, California

A multichannel dielectric-resonator oscillator (DRO), built as a prototype of a local oscillator for an X-band transmitter or receiver, is capable of being electrically tuned among and within 26 adjacent frequency channels, each 1.16 MHz wide, in a band ranging from $\approx 7,040$ to $\approx 7,070$ GHz. The tunability of this oscillator is what sets it apart from other DROs, making it possible to use mass-produced oscillator units of identical design in diverse X-band applications in which there are requirements to use different fixed frequencies or to switch among frequency channels.

The oscillator (see figure) includes a custom-designed voltage-controlled-oscillator (VCO) monolithic microwave integrated circuit (MMIC), a dielectric resonator disk ("puck"), and two varactor-coupling circuits, all laid out on a 25-mil (0.635-mm)-thick alumina substrate having a length and width of 17.8 mm. The resonator disk has a diameter of 8.89 mm and a thickness of 4.01 mm. The oscillator is mounted in an 8.9-mm-deep cavity in a metal housing.

The VCO MMIC incorporates a negative-resistance oscillator amplifier along with a buffer amplifier. The resonator disk is coupled to a microstrip transmission line connected to the negative-resistance port of the VCO MMIC. The two varactor-coupling circuits include microstrip lines, laid out orthogonally to each other, for coupling with the resonator disk. Each varactor microstrip line is DC-coupled to an external port via a microwave choke. One varactor is used for coarse tuning to select a channel; the other varactor is used (1) for fine tuning across the 1.16-MHz width of each channel and (2) as a feedback port for a phase-lock loop. The resonator disk is positioned to obtain (1) the most desir-



Microstrip Lines provide coupling among the resonator disk, the tuning varactors, and the VCO MMIC.

able bandwidth, (2) relatively tight coupling with the microstrip connected to the coarse-tuning varactor, and (3) relatively loose coupling with the microstrip connected to the fine-tuning varactor.

Measurements of performance showed that the oscillator can be switched among any of the 26 channels and can be phase-

locked to a nominal frequency in any channel. The degree of nonlinearity of tuning was found not to exceed 2.5 percent. The tuning sensitivity was found to be 6.15 MHz/V at a bias offset of -2 V on the phase-lock-loop varactor. The phase noise of the oscillator in free-running operation was found to be -107 dBc/Hz (where "dBc" sig-

nifies decibels relative to the carrier signal) at 100 kHz away from the carrier frequency.

This work was done by Narayan Mysoor, Matthew Dennis, and Brian Cook of Caltech for NASA's Jet Propulsion Laboratory. Further information is contained in a TSP (see page 1). NPO-41275

Automatic Alignment of Displacement-Measuring Interferometer

Corrections are derived from fluctuations associated with circular dithering of a laser beam.

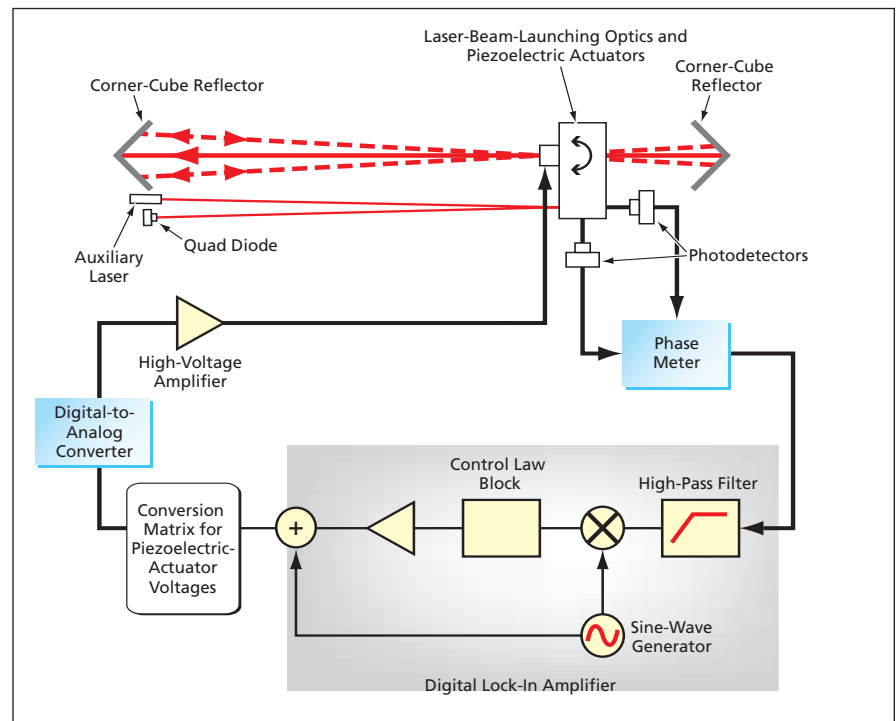
NASA's Jet Propulsion Laboratory, Pasadena, California

A control system strives to maintain the correct alignment of a laser beam in an interferometer dedicated to measuring the displacement or distance between two fiducial corner-cube reflectors. The correct alignment of the laser beam is parallel to the line between the corner points of the corner-cube reflectors: Any deviation from parallelism changes the length of the optical path between the reflectors, thereby introducing a displacement or distance measurement error.

On the basis of the geometrical optics of corner-cube reflectors, the length of the optical path can be shown to be $L = L_0 \cos \theta$, where L_0 is the distance between the corner points and θ is the misalignment angle. Therefore, the measurement error is given by $\Delta L = L_0(\cos \theta - 1)$. In the usual case in which the misalignment is small, this error can be approximated as $\Delta L \approx -L_0 \theta^2 / 2$.

The control system (see figure) is implemented partly in hardware and partly in software. The control system includes three piezoelectric actuators for rapid, fine adjustment of the direction of the laser beam. The voltages applied to the piezoelectric actuators include components designed to scan the beam in a circular pattern so that the beam traces out a narrow cone (60 microradians wide in the initial application) about the direction in which it is nominally aimed. This scan is performed at a frequency (2.5 Hz in the initial application) well below the resonance frequency of any vibration of the interferometer.

The laser beam makes a round trip to both corner-cube reflectors and then interferes with the launched beam. The interference is detected on a photodiode. The length of the optical path is measured by a heterodyne technique: A 100-kHz frequency shift between the launched beam and a reference beam imposes, on the detected signal, an interferometric phase shift proportional to the



This **Simplified Schematic Diagram** of the control system illustrates the control of the tilt of the laser beam about one of two orthogonal tilt axes.

length of the optical path. A phase meter comprising analog filters and specialized digital circuitry converts the phase shift to an indication of displacement, generating a digital signal proportional to the path length.

If the axis of the conical scan is correctly aligned, then the path-length signal is steady and the path-length error remains constant at about $-L_0 \theta_0^2 / 2$, where, in this case, θ_0 is the half cone angle. If, however, the axis of the conical scan is slightly misaligned, then the misalignment angle consists of a steady component θ_0 plus a small fluctuating component $\Delta \theta$. In this case, the optical-path length fluctuates by approximately $-L_0 \theta_0 \Delta \theta$. In a lock-

in amplifier, the digital path-length signal is high-pass-filtered to eliminate the steady component, then the remaining fluctuating component is synchronously demodulated to generate DC signals proportional to the two tilt angles that characterize the misalignment. These signals are superimposed upon the voltages applied to the piezoelectric actuators to counteract the misalignment.

This work was done by Peter Halverson, Martin Regehr, Robert Spero, Oscar Alvarez-Salazar, Frank Loya, and Jennifer Logan of Caltech for NASA's Jet Propulsion Laboratory. Further information is contained in a TSP (see page 1). NPO-40957



🌀 Earth Observing System Data Gateway

The Earth Observing System Data Gateway (EDG) software provides a “one-stop-shopping” standard interface for exploring and ordering Earth-science data stored at geographically distributed sites. EDG enables a user to do the following:

- Search for data according to high-level criteria (e.g., geographic location, time, or satellite that acquired the data);
- Browse the results of a search, viewing thumbnail sketches of data that satisfy the user’s criteria; and
- Order selected data for delivery to a specified address on a chosen medium (e.g., compact disk or magnetic tape).

EDG consists of (1) a component that implements a high-level client/server protocol, and (2) a collection of C-language libraries that implement the passing of protocol messages between an EDG client and one or more EDG servers. EDG servers are located at sites usually called “Distributed Active Archive Centers” (DAACs). Each DAAC may allow access to many individual data items, called “granules” (e.g., single Landsat images). Related granules are grouped into collections called “data sets.” EDG enables a user to send a search query to multiple DAACs simultaneously, inspect the resulting information, select browseable granules, and then order selected data from the different sites in a seamless fashion.

*This program was developed by Robin Pfister of Goddard Space Flight Center and Joe McMahon, James Amrhein, Ed Siefert, Lorena Marsans, Mark Solomon, and Mark Nestler of Global Science & Technology, Inc. Further information is contained in a TSP (see page 1).
GSC-14938-1*

🌀 Power User Interface

Power User Interface 5.0 (PUI) is a system of middleware that is an alternative to the computer program described in the immediately preceding article. Written for expert users in the Earth-science community, PUI enables expedited ordering of data granules on the basis of specific granule-identifying information

that the users already know or can assemble. PUI also enables expert users to perform quick searches for orderable-granule information for use in preparing orders. PUI 5.0 is available in two versions (note: PUI 6.0 has command-line mode only): a Web-based application program and a UNIX command-line-mode client program. Both versions include modules that perform data-granule-ordering functions in conjunction with external systems. The Web-based version works with Earth Observing System Clearing House (ECHO) metadata catalog and order-entry services and with an open-source order-service broker server component, called the Mercury Shopping Cart, that is provided separately by Oak Ridge National Laboratory through the Department of Energy. The command-line version works with the ECHO metadata and order-entry process service. Both versions of PUI ultimately use ECHO to process an order to be sent to a data provider. Ordered data are provided through means outside the PUI software system.

*This program was developed by Robin Pfister of Goddard Space Flight Center and Joe McMahon of Global Science & Technology, Inc. Further information is contained in a TSP (see page 1).
GSC-14939-1*

🌀 Mercury Shopping Cart Interface

Mercury Shopping Cart Interface (MSCI) is a reusable component of the Power User Interface 5.0 (PUI) program described in the immediately preceding article. MSCI is a means of encapsulating the logic and information needed to describe an orderable item consistent with Mercury Shopping Cart service protocol. Designed to be used with Web-browser software, MSCI generates Hypertext Markup Language (HTML) pages on which ordering information can be entered. MSCI comprises two types of Practical Extraction and Report Language (PERL) modules: template modules and shopping-cart logic modules. Template modules generate HTML pages for entering the required ordering details and enable submission of the order via a Hypertext Transfer Protocol (HTTP) post. Shop-

ping-cart modules encapsulate the logic and data needed to describe an individual orderable item to the Mercury Shopping Cart service. These modules evaluate information entered by the user to determine whether it is sufficient for the Shopping Cart service to process the order. Once an order has been passed from MSCI to a deployed Mercury Shopping Cart server, there is no further interaction with the user.

*This program was developed by Robin Pfister of Goddard Space Flight Center and Joe McMahon of Global Science & Technology, Inc. Further information is contained in a TSP (see page 1).
GSC-14940-1*

🌀 Cassini Archive Tracking System

The Cassini Archive Tracking System (CATS) is a computer program that enables tracking of scientific data transfers from originators to the Planetary Data System (PDS) archives. Without CATS, there is no systematic means of locating products in the archive process or ensuring their completeness. By keeping a database of transfer communications and status, CATS enables the Cassini Project and the PDS to efficiently and accurately report on archive status. More importantly, problem areas are easily identified through customized reports that can be generated on the fly from any Web-enabled computer. A Web-browser interface and clearly defined authorization scheme provide safe distributed access to the system, where users can perform functions such as create customized reports, record a transfer, and respond to a transfer. CATS ensures that Cassini provides complete science archives to the PDS on schedule and that those archives are available to the science community by the PDS. The three-tier architecture is loosely coupled and designed for simple adaptation to multi-mission use. Written in the Java programming language, it is portable and can be run on any Java-enabled Web server.

This work was done by Diane Conner, Elias Sayfi, and Adrian Tinio of Caltech for NASA’s Jet Propulsion Laboratory. Further information is contained in a TSP (see page 1).

This software is available for commercial licensing. Please contact Karina Edmonds of the California Institute of Technology at (818) 393-2827. Refer to NPO-40951.

Architecture Adaptive Computing Environment

Architecture Adaptive Computing Environment (aCe) is a software system that includes a language, compiler, and run-time library for parallel computing. aCe was developed to enable programmers to write programs, more easily than was previously possible, for a variety of parallel computing architectures. Heretofore, it has been perceived to be difficult to write parallel programs for parallel computers and more difficult to port the programs to different parallel computing architectures. In contrast, aCe is supportable on all high-performance computing architectures. Currently, it is supported on LINUX clusters. aCe uses parallel programming constructs that facilitate writing of parallel programs. Such constructs were used in single-instruction/multiple-data (SIMD) programming languages of the 1980s, including Parallel Pascal, Parallel Forth, C*, *LISP, and MasPar MPL. In aCe, these constructs are extended and

implemented for both SIMD and multiple-instruction/multiple-data (MIMD) architectures. Two new constructs incorporated in aCe are those of (1) scalar and virtual variables and (2) pre-computed paths. The scalar-and-virtual-variables construct increases flexibility in optimizing memory utilization in various architectures. The pre-computed-paths construct enables the compiler to pre-compute part of a communication operation once, rather than computing it every time the communication operation is performed.

This program was written by John E. Dorband of Goddard Space Flight Center. For further information, contact the Goddard Innovative Partnerships Office at (301) 286-5810. GSC-14911-1

Computing Fault Displacements From Surface Deformations

Simplex is a computer program that calculates locations and displacements of subterranean faults from data on Earth-surface deformations. The calculation involves inversion of a forward model (given a point source representing a fault, a forward model calculates

the surface deformations) for displacements, and strains caused by a fault located in isotropic, elastic half-space. The inversion involves the use of nonlinear, multiparameter estimation techniques. The input surface-deformation data can be in multiple formats, with absolute or differential positioning. The input data can be derived from multiple sources, including interferometric synthetic-aperture radar, the Global Positioning System, and strain meters. Parameters can be constrained or free. Estimates can be calculated for single or multiple faults. Estimates of parameters are accompanied by reports of their covariances and uncertainties. Simplex has been tested extensively against forward models and against other means of inverting geodetic data and seismic observations.

This work was done by Gregory Lyzenga, Jay Parker, and Andrea Donnellan of Caltech and Wendy Panero of Ohio State University for NASA's Jet Propulsion Laboratory. Further information is contained in a TSP (see page 1).

This software is available for commercial licensing. Please contact Karina Edmonds of the California Institute of Technology at (818) 393-2827. Refer to NPO-41078.



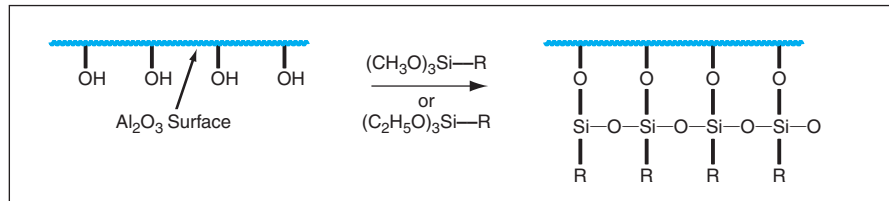
Oxygen-Permeable, Hydrophobic Membranes of Silanized α - Al_2O_3

These membranes perform better than do organic polymer oxygen-diffusion membranes.

Lyndon B. Johnson Space Center, Houston, Texas

Membranes made of silanized alumina have been prepared and tested as prototypes of derivatized ceramic membranes that are both highly permeable to oxygen and hydrophobic. Improved oxygen-permeable, hydrophobic membranes would be attractive for use in several technological disciplines, including supporting high-temperature aqueous-phase oxidation in industrial production of chemicals, oxygenation of aqueous streams for bioreactors, and oxygenation of blood during open-heart surgery and in cases of extreme pulmonary dysfunction. In comparison with organic polymeric oxygen-permeable membranes now commercially available, the derivatized ceramic membranes are more chemically robust, are capable of withstanding higher temperatures, and exhibit higher oxygen-diffusion coefficients.

Membranes made from alumina as well as such other ceramics as titania and zirconia are permeable to oxygen and capable of withstanding higher temperatures. However, without modification, these ceramics are also hydrophilic. Hence, it is necessary to modify the surface properties of these ceramics to ren-



Hydrophobic Groups (R) have been attached to alumina surfaces by silanization. Thus far, four hydrophobic groups have been studied: $\text{R} = -\text{CH}_2-\text{CH}_2-\text{CH}_2-\text{CH}_3$, $\text{R} = -\text{CH}_2-\text{CH}_2(\text{CF}_2)_7\text{CF}_3$, $\text{R} = -(\text{CH}_2)_{11}\text{CH}_3$, and $\text{R} = -(\text{CH}_2)_{17}\text{CH}_3$.

der them hydrophobic. For a series of experiments, the prototype membranes were made from α - Al_2O_3 with pore sizes from 5 to 200 nm. Hydrophobic molecular groups were attached to each α - Al_2O_3 membrane through silanization, using a suitable trimethoxy- or triethoxysilane (see figure).

In the experiments, both the silanized α - Al_2O_3 membranes and an organic polymer membrane based on polydimethylsiloxane (PDMS) were used as media for the transport of oxygen from a constant-pressure gas phase into a recirculating aqueous stream. Coefficients of diffusion of O_2 and H_2O across the membranes were measured. At room temperature, the silanized α - Al_2O_3 membranes exhibited oxygen-diffusion coef-

ficients ranging from 1.24 to 5.75 times that of the PDMS membrane, the value in each case depending on the pore size and on which hydrophobic functional groups were present. Water-loss rates of the silanized α - Al_2O_3 membranes were found to be as much as two orders of magnitude below that of the PDMS membrane. In one test at a temperature of 90 °C, one of the silanized α - Al_2O_3 membranes exhibited an oxygen-diffusion coefficient 23.9 times that of the PDMS membrane at 23 °C.

This work was done by James E. Atwater and James R. Akse of Umpqua Research Co. for Johnson Space Center. For further information, contact the Johnson Innovative Partnerships Office at (281) 483-3809. MSC-23384

SiC Composite Turbine Vanes

Y-cloth was conceived to provide fiber reinforcement for sharp trailing edges.

John H. Glenn Research Center, Cleveland, Ohio

Turbine inlet guide vanes have been fabricated from composites of silicon carbide fibers in silicon carbide matrices. A unique design for a cloth made from SiC fibers makes it possible to realize the geometric features necessary to form these vanes in the same airfoil shapes as those of prior metal vanes.

The fiber component of each of these vanes was made from SiC-fiber cloth coated with boron nitride. The matrix was formed by chemical-vapor infiltra-

tion with SiC, then slurry-casting of SiC, followed by melt infiltration with silicon.

These SiC/SiC vanes were found to be capable of withstanding temperatures 400 °F (222 °C) greater than those that can be withstood by nickel-base-superalloy turbine airfoils now in common use in gas turbine engines. The higher temperature capability of SiC/SiC parts is expected to make it possible to use them with significantly less cooling than is used for metallic parts, thereby enabling

engines to operate more efficiently while emitting smaller amounts of NO_x and CO.

The SiC/SiC composite vanes were fabricated in two different configurations. Each vane of one of the configurations has two internal cavities formed by a web between the suction and the pressure sides of the vane. Each vane of the other configuration has no web (see Figure 1).

It is difficult to fabricate components having small radii, like those of the trail-

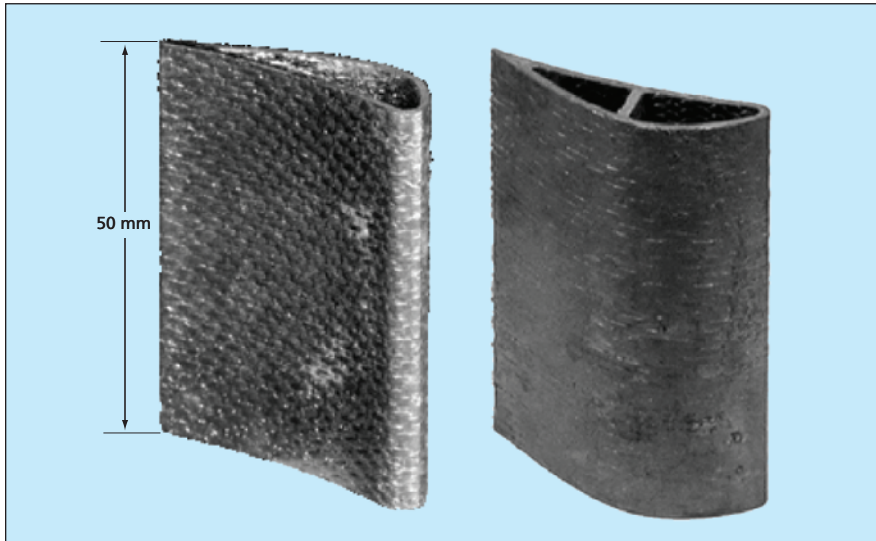


Figure 1. SiC/SiC Composite Turbine Vanes were fabricated in two configurations: one webless, one with an internal web.

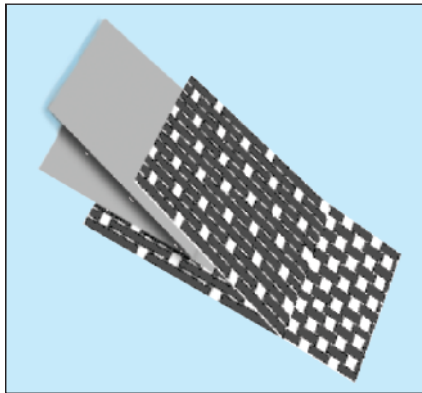


Figure 2. Y-Cloth made it possible to form trailing edges to the required small radius.

ing edges of these vanes, by use of stiff stoichiometric SiC fibers currently preferred for SiC/SiC composites. To satisfy the severe geometric and structural requirements for these vanes, the aforementioned unique cloth design, denoted by the term “Y-cloth,” was

conceived (see Figure 2). In the regions away from the trailing edge, the Y-cloth features a fiber architecture that had been well characterized and successfully demonstrated in combustor liners. To form a sharp trailing edge (having a radius of 0.3 mm), the cloth was split into two planes during the weaving process. The fiber tows forming the trailing-edge section were interlocked, thereby enhancing through-thickness strength of the resulting composite material.

For vanes of the webless configuration, each made from a layup of six plies of Y-cloth, the length of each Y-cloth layer was cut so that the two strips corresponding to the aforementioned two planes would wrap around the perimeter of a graphite vane preform tool with a 10-mm overlap. The overlap was used to join the two strips in a fringe splice. To make the external sixth ply, a standard woven cloth was cut to the required final length and a fringe splice joined the two ends of the

cloth at the trailing edge. The cloth was then prepregged. The entire assembly was then placed into an aluminum compaction tool designed to form the outer net shape of the vane. After the prepreg material was allowed to dry, the preform was removed from the aluminum tooling and placed into an external graphite tool before being shipped to a vendor for matrix infiltration.

To make the SiC fiber preform for a vane having an internal web, a slightly different initial approach was followed. Each of two sections forming the internal cavities (and ultimately the web) was created by first slipping two concentric layers of a two-dimensional, 2-by-2, $\pm 45^\circ$ -braided tube around a net-shape graphite mandrel. The tubes on both mandrels were prepregged and allowed to dry. The resulting two subassemblies were put together, then four additional plies were wrapped around them in the same fashion as that described above for the six plies of the vaneless configuration.

The consolidation of the SiC fiber preforms into SiC/SiC composite parts was performed by commercial vendors using their standard processes. The capability of two of the webless SiC/SiC turbine vanes was demonstrated in tests in a turbine environment. The tests included 50 hours of steady-state operation and 102 two-minute thermal cycles. A surface temperature of 1,320 °C was reached during the tests.

This work was done by Anthony M. Calomino and Michael J. Verrilli of Glenn Research Center. Further information is contained in a TSP (see page 1).

Inquiries concerning rights for the commercial use of this invention should be addressed to NASA Glenn Research Center, Innovative Partnerships Office, Attn: Steve Fedor, Mail Stop 4-8, 21000 Brookpark Road, Cleveland, Ohio 44135. Refer to LEW-17882-1.



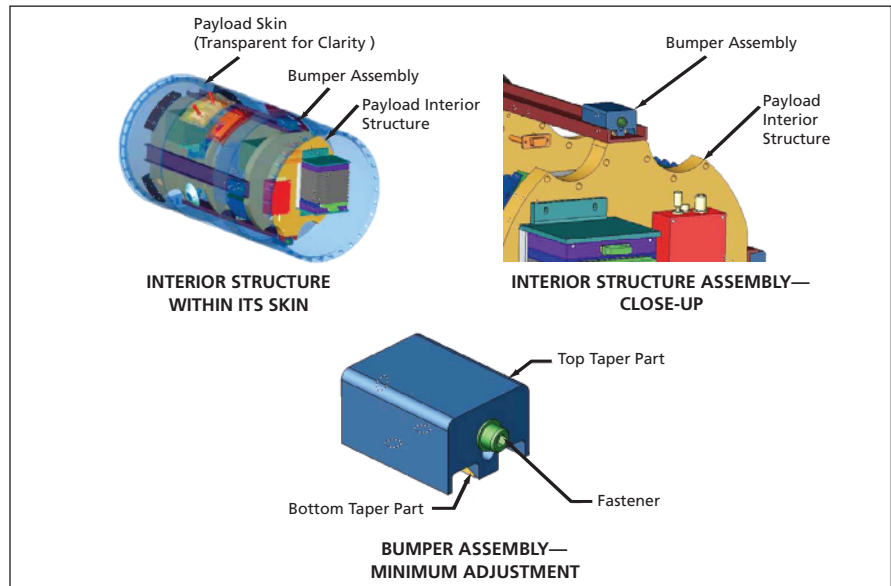
Retaining Device for the Interior Structure of a Spacecraft Payload

Device protects without penalizing interior space.

Goddard Space Flight Center, Greenbelt, Maryland

A device denoted as a bumper assembly for a spacecraft payload container comprises an interior structure surrounded by skin or some other protective enclosure (see figure). When arranged with three or more like assemblies, this bumper assembly is designed to secure the interior structure within a payload's protective enclosure during the stresses endured in flight and, if required, recovery of the payload. Furthermore, proper use of this innovation facilitates the ability of designers and engineers to maximize the total placement area for components, thus increasing utilization of very valuable and limited space.

Typically, the interior structure includes substantially circular decks nominally orthogonal to and centered on the cylindrical axis with the decks connected by axial columns. At one end of the cylinder, the interior structure is attached to the skin by use of fasteners. At other locations, the column portions of the interior structure are connected to the cylindrical skin via four bumper assemblies. The bumper assemblies provide lateral, (that is, radial and circumferential) support while allowing sliding parallel to the cylindrical axis to accommodate axial expansion and contraction. The shape of the interior structure can be varied from the stated "typical" one. The attachment of the end of any interior structure to a protective enclosure, while placing the bumper assemblies in a radial symmetric pattern on the structure's other end,



The **Bumper Assembly** for a spacecraft payload container protects the interior of the payload container, as shown in different magnified views.

would allow similar support during the process of positioning and securing the bumper assemblies.

Each bumper assembly includes two mating wedges held together by a bolt. The bolt is inserted through a clearance hole in one wedge to engage a threaded hole in the other wedge. The positioning and securing of the interior structure can be adjusted by turning the bolt to slide the wedges along their mating sloped surfaces. This arrangement of the interior structure is accomplished

from the structure's outside area and does not require access holes or surfaces machined within its protective enclosure to achieve that accessibility. This accessibility minimizes the time needed to finish the securing of the interior structure within a payload's protective enclosure.

This work was done by Orville N. Fleming, Jr., of Northrop Grumman Corp. for Goddard Space Flight Center. Further information is contained in a TSP (see page 1).

Tool for Torquing Circular Electrical-Connector Collars

A simple tool exerts a strong grip.

Goddard Space Flight Center, Greenbelt, Maryland

An improved tool has been devised for applying torque to lock and unlock knurled collars on circular electrical connectors. The tool was originally designed for, and used by, astronauts working in outer space on the Hubble Space Telescope (HST). The tool is readily adapt-

able to terrestrial use in installing and removing the same or similar circular electrical connectors as well as a wide variety of other cylindrical objects, the tightening and loosening of which entail considerable amounts of torque.

Other tools developed previously for

mating or de-mating electrical connector collars were either designed for use on specific connectors or too generic and incapable of applying the requisite amount of torque [40 lb-in. (4.52 N-m)] for the HST application. In contrast, the present improved tool can be used on a

variety of connector sizes and is capable of applying the requisite amount of torque. Indeed, only a moderate amount of hand clasping force [25 lb (≈ 111 N)] is necessary for applying double the requisite amount of torque.

The tool consists of two stainless steel arms that pivot about a common point. Attached to the gripping jaws on the arms are a total of four flat pads, made of commercially available rubberlike epoxy. The pads make tangential contact with the circular connector collar. Under the gripping force, the pads deform into greater conformity with the gripped ob-

ject and are thereby capable of exerting a greater tangential frictional force. Hence, this jaw-and-pad combination enables the tool to fit circular connectors of different diameters and to exert greater torque than could otherwise be applied. A simple spring-lever resists the user's hand-grasping force with just enough force to return the gripping jaws to the wide-open position.

Although deformation of the pads in repeated use of the tool degrades performance, the amount of degradation may be acceptable in some applications and was acceptable in the original HST

application. In that application, the tool performed as required when used to loosen, then later to tighten, 36 connectors in an operation to remove and replace a power-control unit. Theoretically, the tool could be used to perform the operation a total of five times.

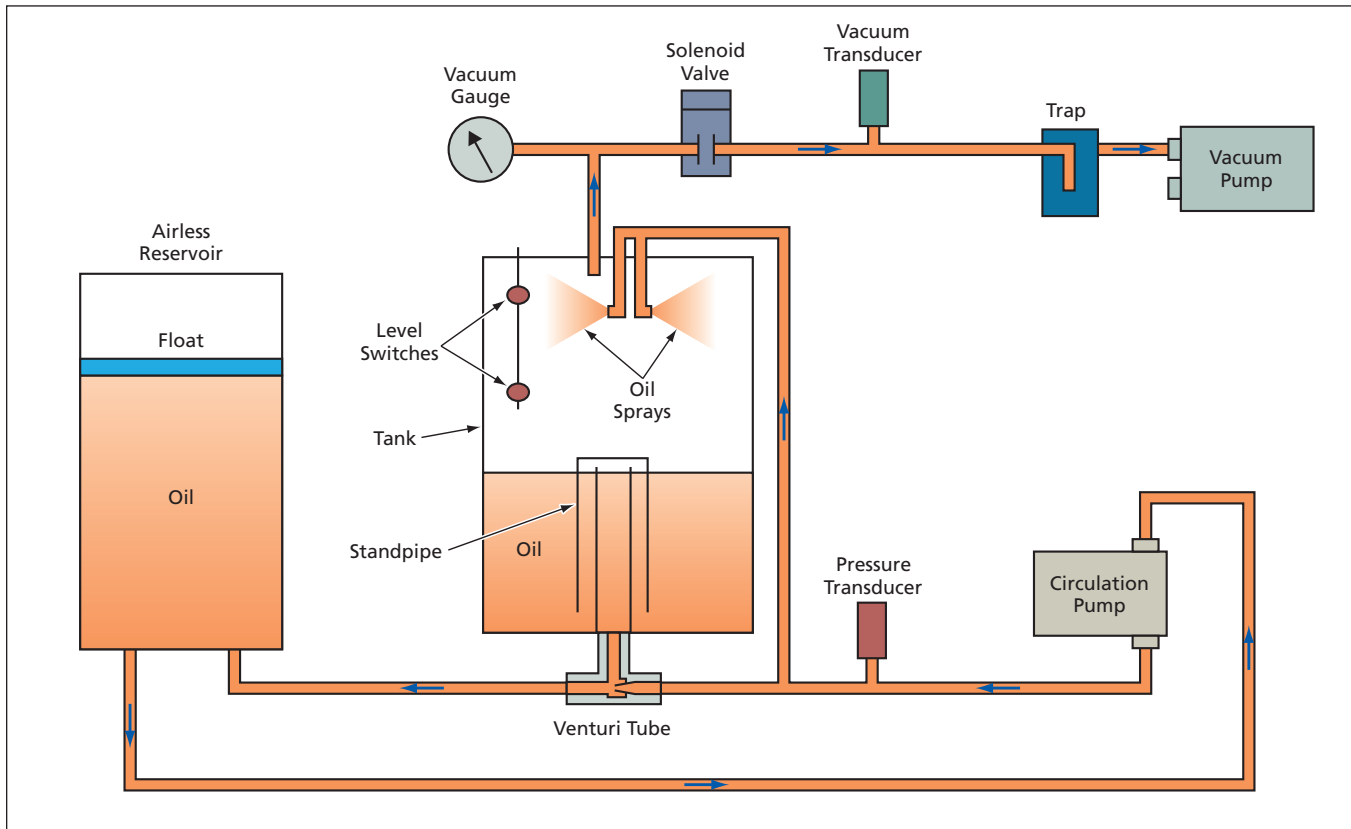
*This work was done by Kathryn Gaulke and Russel Werneth of **Goddard Space Flight Center**, John Grunsfeld of Johnson Space Center, and Patrick O'Neill and Russ Snyder of Swales Aerospace. Further information is contained in a TSP (see page 1). GSC-14670-1*



System for Continuous Deaeration of Hydraulic Oil

The proportion of dissolved air is reliably maintained below 1 volume percent.

John F. Kennedy Space Center, Florida



Oil Is Circulated continuously between the reservoir and the tank. Oil is sprayed in the tank to maximize its exposure to vacuum for rapid removal of dissolved air and water.

A system for continuous, rapid deaeration of hydraulic oil has been built to replace a prior system that effected deaeration more slowly in a cyclic pressure/vacuum process. Such systems are needed because (1) hydraulic oil has an affinity for air, typically containing between 10 and 15 volume percent of air and (2) in the original application for which these systems were built, there is a requirement to keep the proportion of dissolved air below 1 volume percent because a greater proportion can lead to pump cavitation and excessive softness in hydraulic-actuator force-versus-displacement characteristics. In addition to overcoming several deficiencies of the prior deaeration system, the present system removes water from the oil.

The system (see figure) includes a pump that continuously circulates oil

at a rate of 10 gal/min (38 L/min) between an 80-gal (303-L) airless reservoir and a tank containing a vacuum. When the circulation pump is started, oil is pumped, at a pressure of 120 psi (827 kPa), through a venturi tube below the tank with a connection to a standpipe in the tank. This action draws oil out of the tank via the standpipe. At the same time, oil is sprayed into the tank in a fine mist, thereby exposing a large amount of oil to the vacuum. When the oil level in the tank falls below the lower of two level switches, a vacuum pump is started, drawing a hard vacuum on the tank through a trap that collects any oil and water entrained in the airflow. When the oil level rises above higher of the two level switches or when the system is shut down, a solenoid valve between

the tank and the vacuum pump is closed to prevent suction of oil into the vacuum pump.

Critical requirements that the system is designed to satisfy include the following:

- The circulation pump must have sufficient volume and pressure to operate the venturi tube and spray nozzles.
- The venturi tube must be sized to empty the tank (except for the oil retained by the standpipe) and maintain a vacuum against the vacuum pump.
- The tank must be strong enough to withstand atmospheric pressure against the vacuum inside and must have sufficient volume to enable exposure of a sufficiently large amount of sprayed oil to the vacuum.

- The spray nozzles must be sized to atomize the oil and to ensure that the rate of flow of sprayed oil does not exceed the rate at which the venturi action can empty the tank.
 - The vacuum pump must produce a hard vacuum against the venturi tube and continue to work when it ingests some oil and water.
 - Fittings must be made vacuum tight (by use of O-rings) to prevent leakage of air into the system.
- The system is fully automatic, and can be allowed to remain in operation with very little monitoring. It is capable of reducing the air content of the oil from 11 to less than 1 volume percent in about 4 hours and to keep the

water content below 100 parts per million.

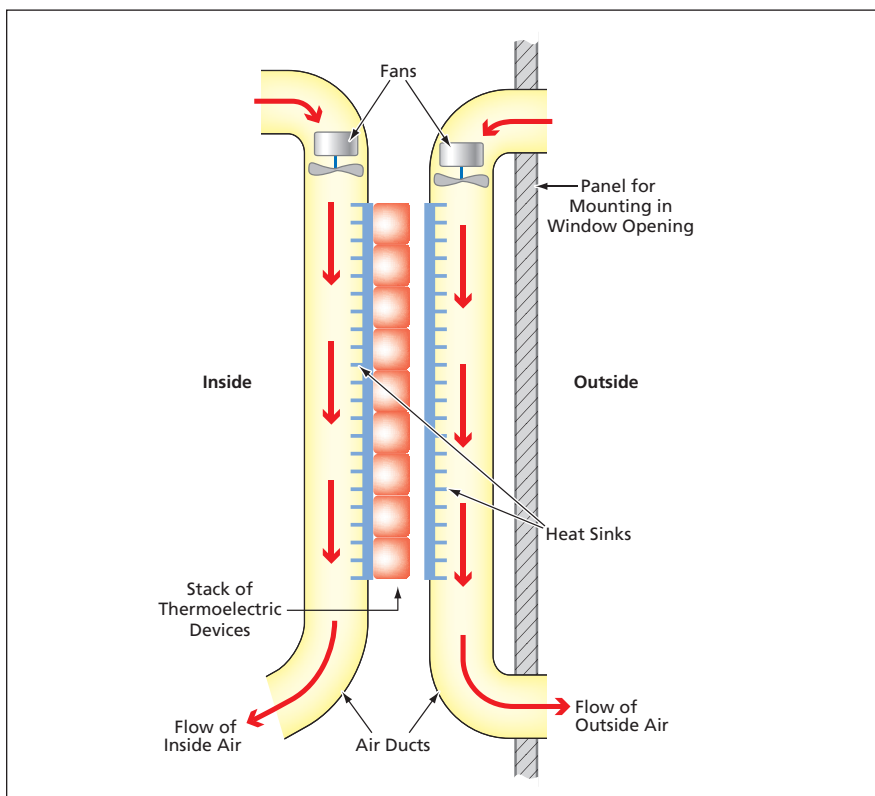
This work was done by Christopher W. Anderson of Lockheed Martin Space Operations for Kennedy Space Center. Further information is contained in a TSP (see page 1).

KSC-12528

⚙️ Solar-Powered Cooler and Heater for an Automobile Interior

Thermoelectric devices and fans would run on solar power.

Marshall Space Flight Center, Alabama



An Assembly Mounted in a Window Opening of an automobile would include thermoelectric devices that would transfer heat between interior and exterior circulating airflows. The thermoelectric devices and the fans in the assembly would be powered by a solar photovoltaic panel mounted on the roof.

The apparatus would include a solar photovoltaic panel mounted on the roof and a panellike assembly mounted in a window opening. The

window-mounted assembly (see figure) would include a stack of thermoelectric devices sandwiched between two heat sinks. A fan would circulate

interior air over one heat sink. Another fan would circulate exterior air over the other heat sink. The fans and the thermoelectric devices would be powered by the solar photovoltaic panel. By means of a double-pole, double-throw switch, the panel voltage fed to the thermoelectric stack would be set to the desired polarity: For cooling operation, the chosen polarity would be one in which the thermoelectric devices transport heat from the inside heat sink to the outside one; for heating operation, the opposite polarity would be chosen.

Because thermoelectric devices are more efficient in heating than in cooling, this apparatus would be more effective as a heater than as a cooler. However, if the apparatus were to include means to circulate air between the outside and the inside without opening the windows, then its effectiveness as a cooler in a hot, sunny location would be increased.

This work was done by Richard T. Howard of Marshall Space Flight Center. Further information is contained in a TSP (see page 1).

This invention has been patented by NASA (U.S. Patent No. 6,662,572). Inquiries concerning nonexclusive or exclusive license for its commercial development should be addressed to Sammy Nabors, MSFC Commercialization Assistance Lead, at sammy.a.nabors@nasa.gov. Refer to MFS-31751-1.



Improved Oxygen-Beam Texturing of Glucose-Monitoring Optics

Textures can be more nearly optimized for greater utilization of light.

John H. Glenn Research Center, Cleveland, Ohio

An improved method has been devised for using directed, hyperthermal beams of oxygen atoms and ions to impart desired textures to the tips of polymethylmethacrylate [PMMA] optical fibers to be used in monitoring the glucose content of blood. The improved method incorporates, but goes beyond, the method described in "Texturing Blood-Glucose-Monitoring Optics Using Oxygen Beams" (LEW-17642-1), *NASA Tech Briefs*, Vol. 29, No. 4 (April 2005), page 11a.

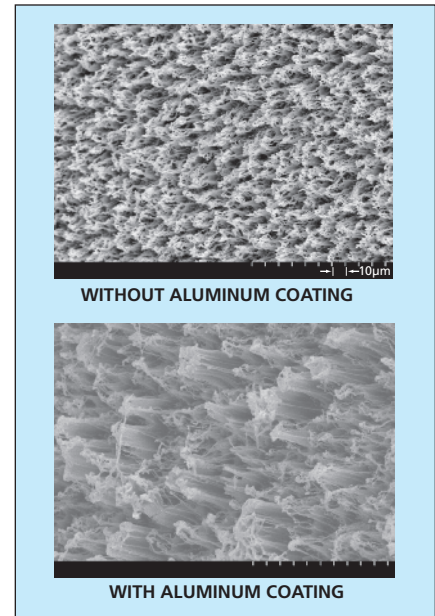
The basic principle of operation of such a glucose-monitoring sensor is as follows: The textured surface of the optical fiber is coated with chemicals that interact with glucose in such a manner as to change the reflectance of the surface. Light is sent down the optical fiber and is reflected from, the textured surface. The resulting change in reflectance of the light is measured as an indication of the concentration of glucose.

The required texture on the ends of the optical fibers is a landscape of microscopic cones or pillars having high aspect ratios (microscopic structures being taller than they are wide). The average distance between hills must be no more than about 5 μm so that blood cells (which are wider) cannot enter the valleys between the hills, where they would interfere with optical sensing of glucose in the blood plasma. On the other hand, the plasma is required to enter the valleys, and high aspect ratio structures are needed to maximize the surface area in contact with the plasma, thereby making it possible to obtain a given level of optical glucose-measurement sensitivity with a relatively small

volume of blood. There is an additional requirement that the hills be wide enough that a sufficient amount of light can propagate into them and, after reflection, can propagate out of them.

The method described in the cited prior article produces a texture comprising cones and pillars that conform to the average-distance and aspect-ratio requirements. However, a significant fraction of the cones and pillars are so narrow that not enough light can propagate along them. The improved method makes it possible to form wider cones and pillars while still satisfying the average-distance and aspect-ratio requirements.

In the improved method, as in the previously reported method, multiple optical fibers are first bundled together for simultaneous texturing of their distal tips. However, prior to texturing by exposure to an oxygen beam, the tips are first coated by vapor deposition of a thin, sparse layer of aluminum: The exposure to the aluminum vapor must be short enough (typically of the order of seconds) so that the aluminum nucleates into islands separated by uncoated areas. The coated tips are textured by exposure to a directed beam of hyperthermal (kinetic energy >1 eV) oxygen atoms and/or ions in a vacuum chamber, as in the previously reported method. The aluminum islands partially shield the underlying PMMA from oxidation and erosion by the beam, so that the cones or pillars remaining after texturing are wider than they would otherwise be. To some extent, the dimensions of the hills and the distances between them can be tailored through choice of the thickness of the alu-



These **Scanning Electron Micrographs** show the results of oxygen-beam texturing of the tips of two PMMA optical fibers: one that was not coated and one that was sparsely coated with aluminum.

minum coat and/or the oxygen-beam fluence. The figure illustrates an example of texturing of the tip of a PMMA optical fiber without and with prior aluminum coating.

This work was done by Bruce A. Banks of Glenn Research Center. Further information is contained in a TSP (see page 1).

Inquiries concerning rights for the commercial use of this invention should be addressed to NASA Glenn Research Center, Innovative Partnerships Office, Attn: Steve Fedor, Mail Stop 4-8, 21000 Brookpark Road, Cleveland, Ohio 44135. Refer to LEW-17975-1.

Tool for Two Types of Friction Stir Welding

The same mechanism could be used for conventional or self-reacting FSW.

Marshall Space Flight Center, Alabama

A tool that would be useable in both conventional and self-reacting friction stir welding (FSW) has been proposed. The tool would embody both a prior

tooling concept for self-reacting FSW and an auto-adjustable pin-tool (APT) capability developed previously as an augmentation for conventional FSW.

Some definitions of terms are prerequisite to a meaningful description of the proposed tool. In conventional FSW, depicted in Figure 1, one uses a tool that

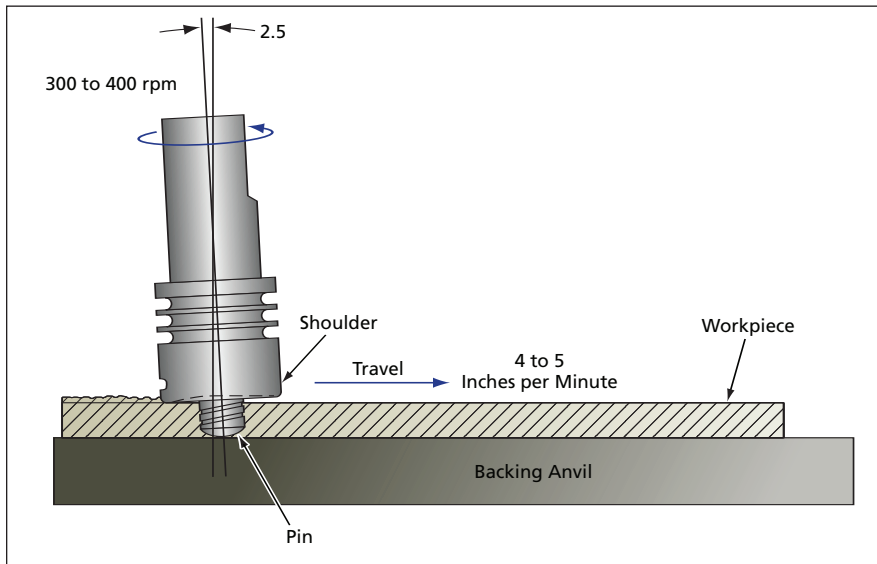


Figure 1. In **Conventional FSW**, the force exerted by the tool on the workpiece is reacted by the backing anvil.

includes (1) a rotating shoulder on top (or front) of the workpiece and (2) a rotating pin that protrudes from the shoulder into the depth of the workpiece. The main axial force exerted by the tool on the workpiece is reacted through a ridged backing anvil under (behind) the workpiece. When conventional FSW is augmented with an APT capability, the depth of penetration of the pin into the workpiece is varied in real time by a position- or force-control system that extends or retracts the pin as needed to obtain the desired effect.

In self-reacting (also known as self-reacted) friction stir welding (SR-FSW), there are two rotating shoulders: one on top (or front) and one on the bottom (or back) of the workpiece. In this case,

a threaded shaft protrudes from the tip of the pin to beyond the back surface of the workpiece. The back shoulder is held axially in place against tension by a nut on the threaded shaft. The main axial force exerted on the workpiece by the tool and front shoulder is reacted through the back shoulder and the threaded shaft, back into the FSW machine head, so that a backing anvil is no longer needed. A key transmits torque between the bottom shoulder and the threaded shaft, so that the bottom shoulder rotates with the shaft. A tool for SR-FSW embodying this concept was reported in "Mechanism for Self-Reacted Friction Stir Welding" (MFS-31914), *NASA Tech Briefs*, Vol. 28, No. 10 (October 2004), page 53.

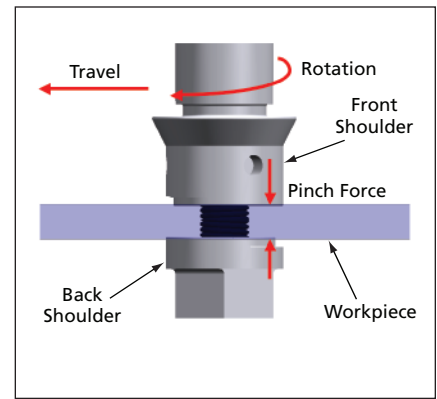


Figure 2. The **Proposed Tool** would include a pin modified to accept a back shoulder.

In its outward appearance, the proposed tool (see Figure 2) would fit the above description of an SR-FSW tool. In this case, the FSW machine would have an APT capability and the pin would be modified to accept a bottom shoulder. The APT capability could be used to vary the distance between the front and back shoulders in real time to accommodate process and workpiece-thickness variations. The tool could readily be converted to a conventional FSW tool, with or without APT capability, by simply replacing the modified pin with a conventional FSW pin.

This work was done by Robert Carter of Marshall Space Flight Center. Further information is contained in a TSP (see page 1).

This invention has been patented by NASA (U.S. Patent No. 6,758,382). Inquiries concerning nonexclusive or exclusive license for its commercial development should be addressed to Sammy Nabors, MSFC Commercialization Assistance Lead, at sammy.a.nabors@nasa.gov. Refer to MFS-31647-1.



Stationary Apparatus Would Apply Forces of Walking to Feet

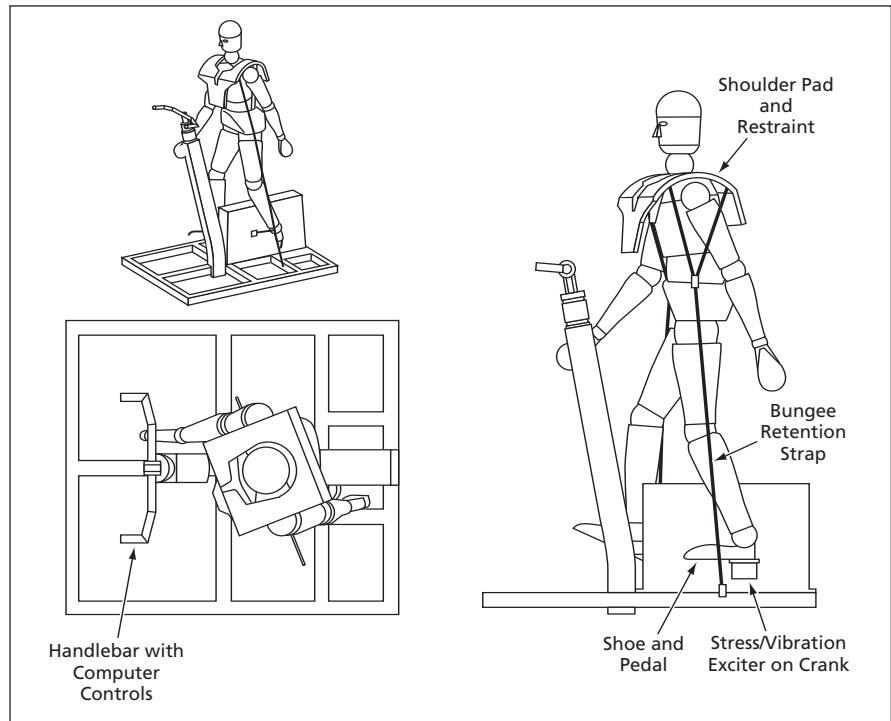
The forces would be tailored to prevent loss of bone density.

Goddard Space Flight Center, Greenbelt, Maryland

A proposed apparatus would apply controlled cyclic forces to both feet for the purpose of preventing the loss of bone density in a human subject whose bones are not subjected daily to the mechanical loads of normal activity in normal Earth gravitation. The apparatus was conceived for use by astronauts on long missions in outer space; it could also be used by bedridden patients on Earth, including patients too weak to generate the necessary forces by their own efforts.

The apparatus (see figure) would be a modified version of a bicyclelike exercise machine, called the cycle ergometer with vibration isolation system (CEVIS), now aboard the International Space Station. Attached to each CEVIS pedal would be a computer-controlled stress/vibration exciter connected to the heel portion of a special-purpose pedal. The user would wear custom shoes that would amount to standard bicycle shoes equipped with cleats for secure attachment of the balls of the feet to the special-purpose pedals.

If possible, prior to use of the apparatus, the human subject would wear a portable network of recording accelerometers, while walking, jogging, and running. The information thus gathered would be fed to the computer, wherein it would be used to make the exciters apply forces and vibrations closely approximating the forces and vibrations experienced by that individual during normal exercise. It is anticipated that like the forces applied to bones during natural exercise,



An Exercise Machine would include computer-controlled stress-vibration exciters that would apply forces substituting for normal exercise forces to stimulate bones.

these artificial forces would stimulate the production of osteoblasts (bone-forming cells), as needed to prevent or retard loss of bone mass.

In addition to helping to prevent deterioration of bones, the apparatus could be used in treating a person already suffering from osteoporosis. For this purpose, the magnitude of the applied forces could be reduced, if necessary, to a level

at which weak hip and leg bones would still be stimulated to produce osteoblasts without exposing them to the full stresses of walking and thereby risking fracture.

This work was done by Jessica Hauss, John Wood, Jason Budinoff, and Michael Correia of Goddard Space Flight Center and Rudolf Albrecht of ESA. Further information is contained in a TSP (see page 1). GSC-14700-1

Instrument Would Detect and Collect Biological Aerosols

Samples would be quickly collected on substrates that would be analyzed automatically.

Marshall Space Flight Center, Alabama

A proposed compact, portable instrument would sample micron-sized airborne particles, would discriminate between biological ones (e.g., bacteria) and nonbiological ones (e.g., dust particles), and would collect the detected bi-

ological particles for further analysis. The instrument is intended to satisfy a growing need for means of rapid, inexpensive collection of bioaerosols in a variety of indoor and outdoor settings. Purposes that could be served by such

collection include detecting airborne pathogens inside buildings and their ventilation systems, measuring concentrations of airborne biological contaminants around municipal waste-processing facilities, monitoring airborne

effluents from suspected biowarfare facilities, and warning of the presence of airborne biowarfare agents.

The instrument would be based partly on a conventional aerosol-particle counter and partly on a fluorescence subsystem for identifying biological particles. Aerosol particles would be drawn through a series of aerodynamic lenses (nozzles sized and shaped to focus variously sized particles into a narrow stream). The lenses would be designed so that only respirable particles would end up in a narrow outlet stream flowing across the optical path of a pulsed ultraviolet laser in the fluorescence-based subsystem. Before reaching the optical path

of the pulsed ultraviolet laser, the aerosol particles would cross the beam of a continuous-wave semiconductor diode laser that would be used to size the particles. If the size of an individual particle was found to be within a certain range, the ultraviolet laser would be triggered to fire as the particle crossed its path, thereby dramatically reducing power requirements for autonomous operation.

The pulse of ultraviolet light would excite fluorescence in the particle. The fluorescent light would be collected and split into three separate spectral bands by use of lenses, dichroic filters, and band-pass filters. The outputs of photodetectors for the three spectral bands

would be processed to determine whether the particle could be of biological origin. The indication of a possible biological particle would cause an aerosol-sampling module to be turned on to collect particles on a solid substrate. The substrate would be placed under an automated microscope equipped with a video camera, the output of which would be digitized and processed by image-analysis software to identify the collected particles.

*This work was done by Steve Savoy and Mike Mayo of Nanohmics, Inc. for **Marshall Space Flight Center**. Further information is contained in a TSP (see page 1). MFS-32081-1*



Boundary Condition for Modeling Semiconductor Nanostructures

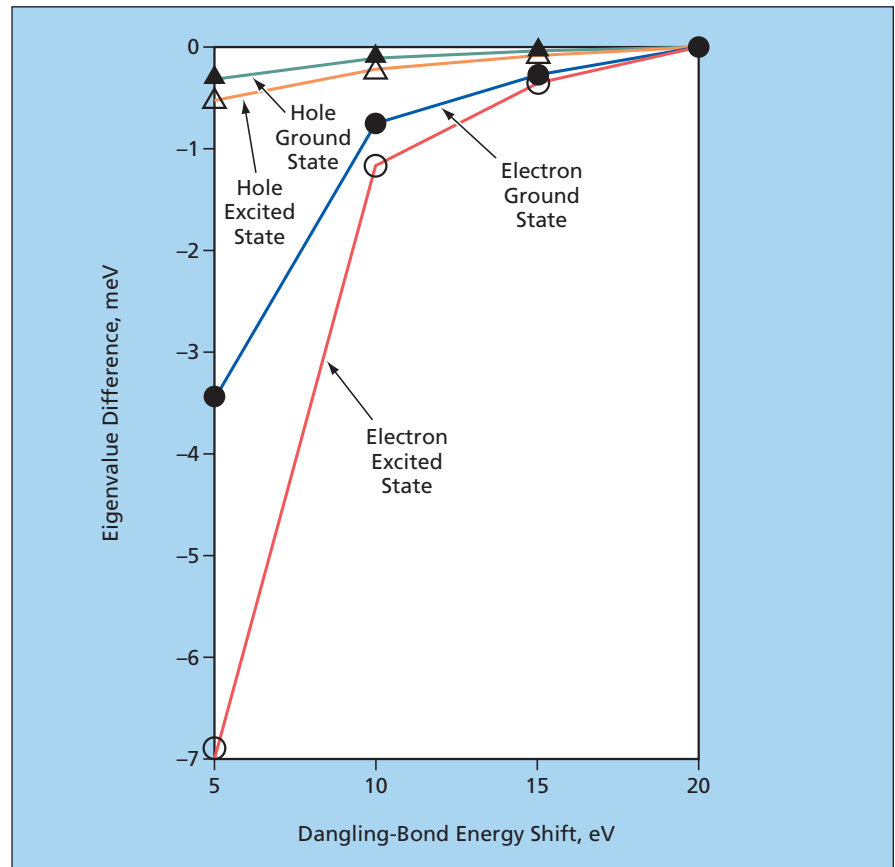
Simulation domains are truncated without introducing spurious surface quantum states.

NASA's Jet Propulsion Laboratory, Pasadena, California

A recently proposed boundary condition for atomistic computational modeling of semiconductor nanostructures (particularly, quantum dots) is an improved alternative to two prior such boundary conditions. As explained below, this boundary condition helps to reduce the amount of computation while maintaining accuracy.

The electronic properties of semiconductor nanostructures (hereafter called “nanodevices”) are already utilized in sensors, lasers, memory circuits, and electro-optical and optoelectronic devices. The electronic properties of a nanodevice are sensitive to numerous parameters, including those pertaining to sizes, shapes, alloy compositions, and interfaces between different materials. Atomistic computational simulation of a nanodevice can help in the selection of optimal parameters in the huge design space inhabited by the parameters. However, until now, the computational burden posed by the large numbers of atoms in a nanodevice has made it necessary to limit computational modeling to a semi-classical, continuum approximation. The purpose served by the present boundary condition (and by the two prior boundary conditions with which the present boundary condition is compared) is to enable truncation of the simulation domain at an artificial boundary surface so that the domain can be made small enough that atomistic computational simulation becomes practical.

The truncation problem can be summarized as follows: Whereas, as its name suggests, a nanodevice can have characteristic dimensions of the order of nanometers, it is typically embedded within a larger semiconductor structure having characteristic dimensions of the order of micrometers. Therefore, in the absence of a means of truncation, the simulation domain must typically encompass all of the atoms contained within a micrometer-sized region. The key to truncation lies in recognition that a smaller electronically active region is



Eigenvalues of Quantum States in the band gap of a simulated InAs-in-GaAs quantum dot are already converged within a few meV at a dangling-bond shift of 5 eV, and converge further as the dangling-bond shift is increased to 20 eV.

defined by localization of the electron density in and near a potential well established by the energy-band offset between two adjacent semiconductor materials. However, without a proper boundary condition, simply drawing an artificial boundary surface around the electronically active region results in many spurious quantum states associated with dangling interatomic bonds at the boundary surface.

The present boundary condition effectively eliminates the spurious surface quantum states by artificially shifting their energy levels well above the energy band of interest, as though the dangling bonds were passivated by high-energy molecules. The size of the dangling-bond energy shift is not critical, as long

as it suffices to remove all spurious quantum states from the semiconductor band gap in the electronically active region of interest. For example, in the case of an InAs self-assembled quantum dot embedded in GaAs, a shift of 5 eV is sufficient to remove the spurious states and make electron and hole energies converge to within a few meV (see figure).

The present boundary condition is a refined version of one of the two prior boundary conditions in which the orbital energies of surface atoms are raised. Whereas the prior boundary condition does not differentiate among such details of the surface atoms as the numbers and directions of their dangling bonds, the present boundary condition does. The present boundary con-

dition is more physically realistic because, unlike in the prior boundary condition, the connected-bond energy of the surface atoms is kept unchanged and, hence, there is no extra energy penalty for electrons to occupy the con-

nected bonds of surface atoms. The other prior boundary condition is a periodic one and, hence, not well suited to modeling a nanodevice that has an irregular shape or is subjected to a non-periodic externally applied potential.

This work was done by Seungwon Lee, Fabiano Oyafuso, Paul von Allmen, and Gerhard Klimeck of Caltech for NASA's Jet Propulsion Laboratory. Further information is contained in a TSP (see page 1). NPO-41155

Miniature Distillation Column for Producing LOX From Air

This column is only about a hundredth as high as an industrial one.

John H. Glenn Research Center, Cleveland, Ohio

The figure shows components of a distillation column intended for use as part of a system that produces high-purity liquid oxygen (LOX) from air by distillation. (The column could be easily modified to produce high-purity liquid nitrogen.) Whereas typical industrial distillation columns for producing high-purity liquid oxygen and/or nitrogen are hundreds of feet tall, this distillation column is less than 3 ft (less than about 0.9 m) tall. This column was developed to trickle-charge a LOX-based emergency oxygen system (EOS) for a large commercial aircraft.

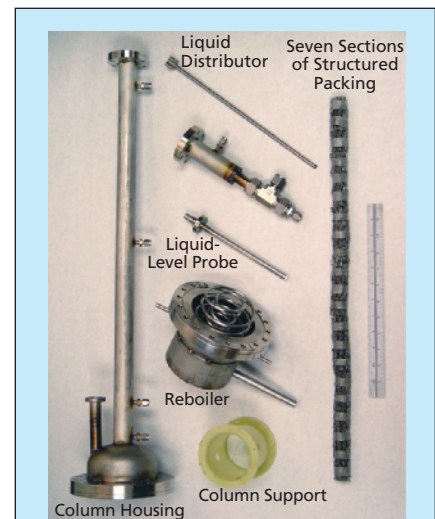
A description of the industrial production of liquid oxygen and liquid nitrogen by distillation is prerequisite to a meaningful description of the present miniaturized distillation column. Typically, such industrial production takes place in a chemical processing plant in which large quantities of high-pressure air are expanded in a turboexpander to (1) recover a portion of the electrical power required to compress the air and (2) partially liquefy the air. The resulting two-phase flow of air is sent to the middle of a distillation column. The liquid phase is oxygen-rich, and its oxygen purity increases as it flows down the column. The vapor phase is nitrogen-rich and its nitrogen purity increases as it flows up the column. A heater or heat exchanger, commonly denoted a reboiler, is at the bottom of the column. The reboiler is so named because its role is to reboil some of the liquid oxygen collected at the bottom of the column to provide a flow of oxygen-rich vapor. As the oxygen-rich vapor flows up the column, it absorbs the nitrogen in the down-flowing liquid by mass transfer. Once the vapor leaves the lower portion of the column, it interacts with down-flowing nitrogen liquid that has been condensed in a heat exchanger, commonly denoted a condenser, at the top of the column. Liquid oxygen and liquid nitrogen products are obtained by

draining some of the purified product at the bottom and top of the column, respectively.

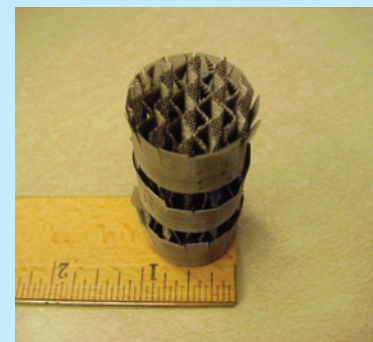
Because distillation is a mass-transfer process, the purity of the product(s) can be increased by increasing the effectiveness of the mass-transfer process (increasing the mass-transfer coefficient) and/or by increasing the available surface area for mass transfer through increased column height. The diameter of a distillation column is fixed by pressure-drop and mass-flow requirements. The approach taken in designing the present distillation column to be short yet capable of yielding a product of acceptably high purity was to pay careful attention to design details that affect mass-transfer processes.

The key components in this column are the structured packing and the distributor. The structured packing is highly compact. Each section of packing is about 1 in. (about 2.5 cm) in diameter and 3 in. (about 7.6 cm) long. The column contains a total of seven sections of packing, so the total length of packing in the column is 21 in. (about 53 cm). The packing promotes transfer of mass between the up-flowing vapor and the down-flowing liquid. The liquid distributor, as its name suggests, helps to distribute the liquid as nearly evenly as possible throughout the cross section of the column so as to utilize the packing to the fullest extent possible and thereby maximize the mass-transfer effectiveness of the column.

In operation, saturated air at a pressure of 70 psia (absolute pressure of 0.48 MPa) enters the reboiler and partially condenses. The air is then fully condensed by an external refrigeration source, such as a small cryocooler. The air then goes through a pressure drop of about 50 psi (about 0.34 MPa) in a throttling valve and thereby becomes partially vaporized. This pressure drop sets the column pressure at about 20 psia (about 0.14 MPa). This column pressure is required to obtain a signifi-



COMPONENTS OF DISTILLATION COLUMN



MAGNIFIED VIEW OF ONE SECTION OF STRUCTURED PACKING

The Components of the Distillation Column are designed to maximize mass transfer in a small space.

cant temperature difference in the reboiler. The two-phase flow then enters a separator, where the vapor is vented, and the liquid is sent to the distributor. Once operation has reached a steady state, mass transfer between the down-flowing liquid and the up-flowing vapor

results in the collection of 99-percent-pure LOX in the reboiler. The nitrogen-rich vapor is vented as waste at the top of the column. The structured packing enables the column operation to be insensitive to tilt angles of up to 20°, with respect to the local gravity vector. We

are currently working to further miniaturize the distillation technology to provide a portable, lightweight, and low-power source of high-purity nitrogen and oxygen for other applications.

This work was done by Jay C. Rozzi of Create, Inc., for Glenn Research Center.

Inquiries concerning rights for the commercial use of this invention should be addressed to NASA Glenn Research Center, Commercial Technology Office, Attn: Steve Fedor, Mail Stop 4-8, 21000 Brookpark Road, Cleveland, Ohio 44135. Refer to LEW-17593-1.

Even Illumination From Fiber-Optic-Coupled Laser Diodes

Emerging light beams would be shaped by diffractive fiber-optic tips.

Marshall Space Flight Center, Alabama

A method of equipping fiber-optic-coupled laser diodes to evenly illuminate specified fields of view has been proposed. The essence of the method is to shape the tips of the optical fibers into suitably designed diffractive optical elements. One of the main benefits afforded by the method would be more nearly complete utilization of the available light.

As shown in Figure 1, the light beam emerging from the flat tip of an optical fiber coupled to a laser diode has a Gaussian distribution of intensity across a circular cross section, whereas what is typically desired is to concentrate the light into a beam characterized by a “top-hat” distribution (even illumination in a specified field of view, zero illumination outside the field of view). In order to obtain an acceptably close approximation of even illumination in the field of view, the Gaussian beam must be significantly wider, so that much or most of the light is wasted outside the field of view. A conventional lens can be used to partially shape the beam, but the beam does not lose its basic Gaussian character; this is true whether the lens is placed at a focal distance from the tip, in contact with the tip, or formed onto the tip surface as an integral part of the optical fiber.

Diffractive optics is a relatively new field of optics in which laser beams are shaped by use of diffraction instead of refraction. There exist ways to produce diffractive lens elements that shape laser beams into desired arbitrary cross sections (for example, the arrow shapes of the beams generated by many laser pointers). In a fiber-optic-coupled laser diode according to the proposal, the optical fiber would be tipped with a diffractive surface such that the diffraction pattern imposed on light leaving the fiber would, at a desired distance from the tip, concentrate the beam at nearly even intensity into a cross section of specified shape.

Usually, the desired illuminated area would be rectangular or circular, but in principle, the diffractive surface could be designed to shape the beam to almost any specified cross section. In one version of the proposal, the diffractive shape would be etched directly onto the initially flat tip surface of the fiber. In another version, the diffractive surface would be molded onto a transparent piece of plastic that would be bonded to the tip, the mold having been previously etched or otherwise formed to the diffractive shape.

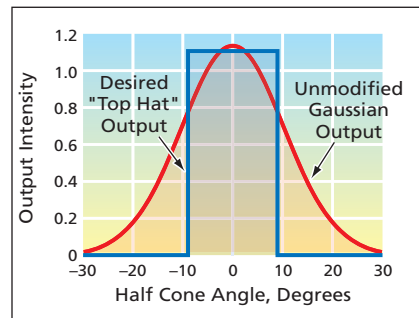


Figure 1. The Distribution of Laser Light emerging from an optical fiber is typically Gaussian, whereas often a “top hat” distribution is desired.

A diffractive fiber-tip surface that would function in this way has not yet been designed. However, it has been estimated, for example, that such a pattern on the tip of an optical fiber of 110- μm diameter would consist of about 300 prisms of various heights resembling buildings on 5- μm -square city blocks (see Figure 2), fabricated by etching the square areas to different depths from an initial flat tip surface. A small developmental problem is posed by the difficulty of etching such a pattern.

As in the case of any diffractive optic, some light would pass through undiffracted; hence, the output light pattern that would be mostly the desired pattern with a slight superimposed Gaussian pattern.

This work was done by Richard T. Howard of Marshall Space Flight Center. Further information is contained in a TSP (see page 1).

This invention is owned by NASA, and a patent application has been filed. For further information, contact Sammy Nabors, MSFC Commercialization Assistance Lead, at sammy.a.nabors@nasa.gov. Refer to MFS-31843-1.

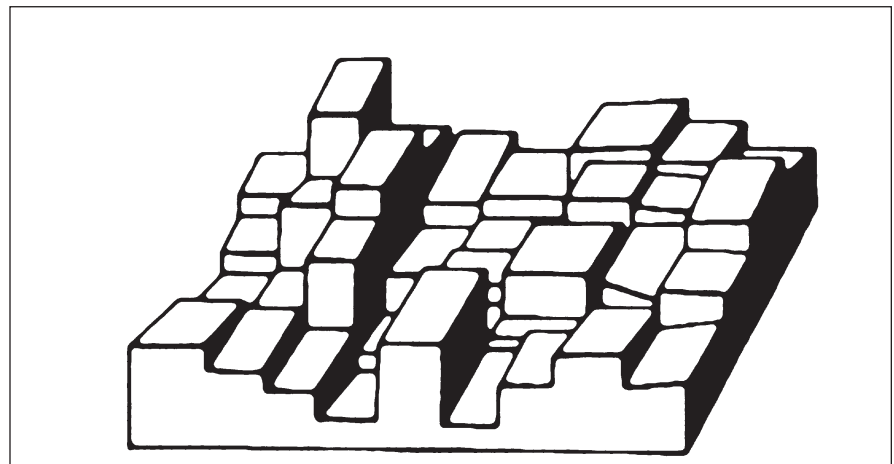


Figure 2. This Diffractive Optic was formed in plastic. Optical performance is affected by the widths and depths of steps and the sharpness of edges. Although a rectangular floor plan is shown in this example, the floor plan for application to the tip of a round optical fiber would be circular, even if the optic were to be used to illuminate a rectangular area.

Optically Driven Deformable Mirrors

There is no wiring on the back sides of these mirrors.

NASA's Jet Propulsion Laboratory, Pasadena, California

Optically driven deformable mirrors may eventually supplant electrically driven deformable mirrors in some adaptive-optics and active-optics applications. Traditionally, the mirror facets in electrically driven deformable mirrors are actuated, variously, by means of piezoelectric, electrostrictive, microelectromechanical, liquid-crystal, or thermal devices. At least one such device must be dedicated to each facet, and there must be at least one wire carrying a control or drive signal to the device. If a deformable mirror comprises many (e.g., thousands) of facets, then wiring becomes a major problem for design, and the problem is compounded in cases of piezoelectric or other actuators for which high drive voltages are required. In contrast, in optically driven mirrors, the wiring problem is eliminated.

The basic principle of actuation of an optically driven deformable mirror is to use a laser beam to actuate a material. For example, a laser beam can be used to heat a material to make the material thermally expand to displace a mirror facet. In an experiment to demonstrate this principle, the actuator was a Golay cell (see Figure 1) having a diameter of ≈ 6 mm and a length of ≈ 10 mm. The beam from a laser diode was aimed at an absorber in the cell, thereby heating the gas in the cell. A mirror mounted on a 12.5- μm -thick polyethylene terephthalate diaphragm at one end of the cell became

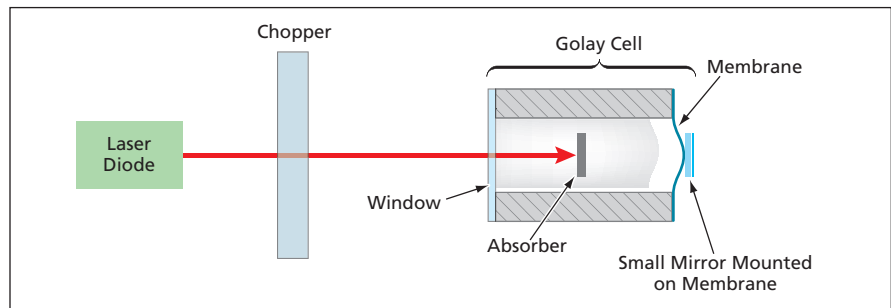


Figure 1. Light From a Laser Diode impinges on an absorber in a Golay cell, heating the gas in the cell. A mirror on the diaphragm is displaced by the resulting expansion of the gas.

displaced as the gas expanded against the diaphragm. In one representative pair of experiments at a laser beam power of 0.23 W, the beam was mechanically chopped at frequencies of 1 and 5 Hz. The mirror exhibited corresponding oscillating displacements having amplitudes of 373 and 83 μm , respectively.

Figure 2 depicts a simple experimental deformable mirror comprising a 5 \times 5 square array of Golay cells with square mirror facets mounted on their membranes. A typical practical deformable mirror would likely include a much larger array (e.g., 100 \times 100). In the contemplated use of such an array, two computer-controlled single-axis mirrors would be used to raster-scan a laser beam across the array, and the raster scan would be synchronized with an amplitude modulation to control the amount of

heat delivered to each cell and thereby to control the displacement of each facet.

This work was done by Hamid Hemmati and William Farr of Caltech for NASA's Jet Propulsion Laboratory. Further information is contained in a TSP (see page 1).

In accordance with Public Law 96-517, the contractor has elected to retain title to this invention. Inquiries concerning rights for its commercial use should be addressed to:

*Innovative Technology Assets Management
JPL*

*Mail Stop 202-233
4800 Oak Grove Drive
Pasadena, CA 91109-8099
(818) 354-2240*

E-mail: iaoffice@jpl.nasa.gov

Refer to NPO-42724, volume and number of this NASA Tech Briefs issue, and the page number.



Algorithm for Automated Detection of Edges of Clouds

The algorithm has been shown to be reliable and robust.

John F. Kennedy Space Center, Florida

An algorithm processes cloud-physics data gathered *in situ* by an aircraft, along with reflectivity data gathered by ground-based radar, to determine whether the aircraft is inside or outside a cloud at a given time. A cloud edge is deemed to be detected when the in/out state changes, subject to a hysteresis constraint. Such determinations are important in continuing research on relationships among lightning, electric charges in clouds, and decay of electric fields with distance from cloud edges.

More specifically, the algorithm consists of an in-cloud detection component and a boundary detection component. The in-cloud detection component relies on the cloud-physics and weather-radar data to make a tentative determination of the in/out state. The boundary detection component examines the output of the in-cloud detection component and applies a hysteresis test, which helps prevent false boundary detections that would otherwise be triggered by momentary data fluctuations associated with isolated transient cloud puffs or data dropouts.

The algorithm was tested by applying it to a large set of data and comparing the results of the algorithm with results obtained through detailed manual examination of the data. The algorithm was found to be highly reliable and insensitive to transient instrumentation noise or data gaps, and it enabled full automation of detection of cloud edges.

This work was done by Jennifer G. Ward and Francis J. Merceret of Kennedy Space Center. Further information is contained in a TSP (see page 1)..
KSC-12574

Exploiting Quantum Resonance to Solve Combinatorial Problems

NASA's Jet Propulsion Laboratory, Pasadena, California

Quantum resonance would be exploited in a proposed quantum-computing approach to the solution of combinatorial optimization problems. In quantum computing in general, one takes advantage of the fact that an algorithm cannot be decoupled from the physical effects available to implement it. Prior approaches to quantum computing have involved exploitation of only a subset of known quantum physical effects, notably including parallelism

and entanglement, but not including resonance. In the proposed approach, one would utilize the combinatorial properties of tensor-product decomposability of unitary evolution of many-particle quantum systems for physically simulating solutions to NP-complete problems (a class of problems that are intractable with respect to classical methods of computation). In this approach, reinforcement and selection of a desired solution would be executed by

means of quantum resonance. Classes of NP-complete problems that are important in practice and could be solved by the proposed approach include planning, scheduling, search, and optimal design.

This work was done by Michail Zak and Amir Fijany of Caltech for NASA's Jet Propulsion Laboratory. Further information is contained in a TSP (see page 1).
NPO-41902

Hybrid Terrain Database

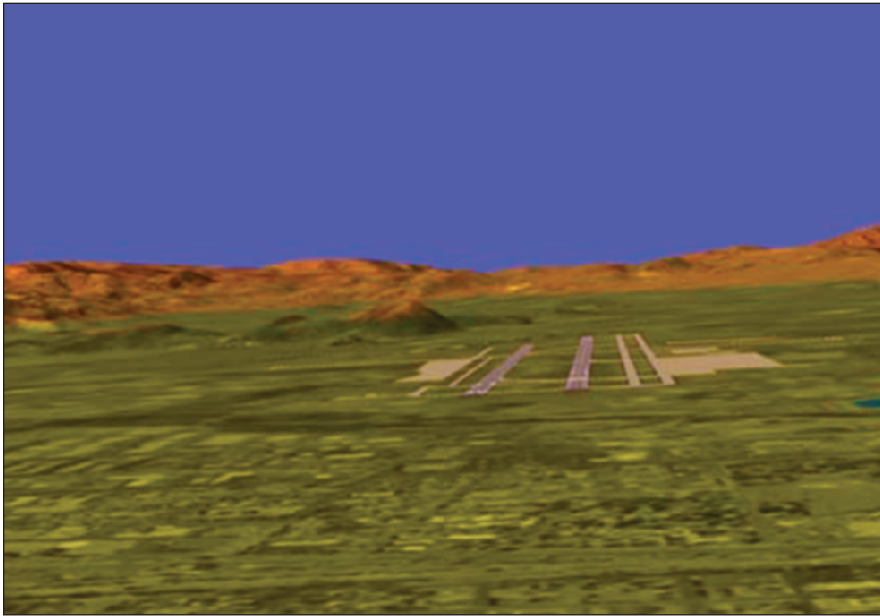
Aerial photographs are draped onto digital elevation maps.

Langley Research Center, Hampton, Virginia

A prototype hybrid terrain database is being developed in conjunction with other databases and with hardware and software that constitute subsystems of aerospace cockpit display systems (known in the art as synthetic vision systems) that generate images to increase

pilots' situation awareness and eliminate poor visibility as a cause of aviation accidents. The basic idea is to provide a clear view of the world around an aircraft by displaying computer-generated imagery derived from an onboard database of terrain, obstacle, and airport information.

The hybrid terrain database, which could constitute all or part of such an onboard database, can be characterized as an accurate model of terrain and obstacles of interest to a pilot. The hybrid terrain database contains (1) imagery derived from conventional aerial photo-



This **Hybrid Textured Terrain** image was generated from a hybrid terrain database of Reno-Tahoe International Airport and its environs.

graphs of a terrain area of interest, (2) a digital elevation map of the terrain area of interest, and, optionally, (3) information on the area of interest from other databases.

The hybrid terrain database is used to generate synthetic terrain imagery (see figure) in a hybrid textured format, which is best described in terms of the process by which the synthetic imagery is generated: The hybrid texture is created from monochromatic aerial photographs of the affected terrain area merged with color-coded elevation-based terrain imagery (see figure). The process involves coloring the monochromatic aerial photographs of the affected area on the basis of altitude and draping the resulting elevation-colored photographs onto the digital elevation model of the terrain.

*This work was done by Trey Arthur of **Langley Research Center**. Further information is contained in a TSP (see page 1).
LAR-16898-1*



✚ On Release of Microbe-Laden Particles From Mars Landers

A paper presents a study in which rates of release of small particles from Mars lander spacecraft into the Martian atmosphere were estimated from first principles. Because such particles can consist of, or be laden with, terrestrial microbes, the study was undertaken to understand their potential for biological contamination of Mars. The study included taking account of forces and energies involved in adhesion of particles and of three mechanisms of dislodgement of particles from the surface of a Mars lander: wind shear, wind-driven impingement of suspended dust, and impingement of wind-driven local saltating sand particles. Wind shear was determined to be effective in dislodging only particles larger than about 10 microns and would probably be of limited interest because such large particles could be removed by pre-flight cleaning of the spacecraft, and their number on the launched spacecraft would thus be relatively small. Dislodgement by wind-driven dust was found to be characterized by an adhesion half-life of the order of 10,000 years — judged to be too long to be of concern. Dislodgement by saltating sand particles, including skirts of dust devils, was found to be of potential importance, depending on the sizes of the spacecraft-attached particles and characteristics of both Mars sand-particle and spacecraft surfaces.

This work was done by Josette Bellan and Kenneth Harstad of Caltech for NASA's Jet Propulsion Laboratory. Further information is contained in a TSP (see page 1). NPO-42687

🔍 A Concept for Run-Time Support of the Chapel Language

A document presents a concept for run-time implementation of other concepts embodied in the Chapel programming language. (Now undergoing development, Chapel is intended to become a standard language for parallel computing that would surpass older such languages in both computational performance in the efficiency with which pre-existing code can be reused and new

code written.) The aforementioned other concepts are those of distributions, domains, allocations, and access, as defined in a separate document called “A Semantic Framework for Domains and Distributions in Chapel” and linked to a language specification defined in another separate document called “Chapel Specification 0.3.” The concept presented in the instant report is recognition that a data domain that was invented for Chapel offers a novel approach to distributing and processing data in a massively parallel environment. The concept is offered as a starting point for development of working descriptions of functions and data structures that would be necessary to implement interfaces to a compiler for transforming the aforementioned other concepts from their representations in Chapel source code to their run-time implementations.

This work was done by Mark James of Caltech for NASA's Jet Propulsion Laboratory. Further information is contained in a TSP (see page 1).

The software used in this innovation is available for commercial licensing. Please contact Karina Edmonds of the California Institute of Technology at (626) 395-2322. Refer to NPO-42496.

🔍 Thermoelectric Inhomogeneities in $(\text{Ag}_{1-y}\text{SbTe}_2)_x(\text{PbTe})_{1-x}$

A document presents a study of why materials of composition $(\text{Ag}_{1-y}\text{SbTe}_2)_{0.05}(\text{PbTe})_{0.95}$ [$0 \leq y \leq 1$] were previously reported to have values of the thermoelectric figure of merit [ZT (where $Z \equiv \alpha^2/\rho\kappa$, α is the Seebeck coefficient, ρ is electrical resistivity, κ is thermal conductivity, and T is absolute temperature)] ranging from <1 to >2 . In the study, samples of $(\text{AgSbTe}_2)_{0.05}(\text{PbTe})_{0.95}$, $(\text{Ag}_{0.67}\text{SbTe}_2)_{0.05}(\text{PbTe})_{0.95}$, and $(\text{Ag}_{0.55}\text{SbTe}_2)_{0.05}(\text{PbTe})_{0.95}$ were prepared by melting followed, variously, by slow or rapid cooling. Analyses of these samples by x-ray diffraction, electron microscopy, and scanning-microprobe measurements of the Seebeck coefficient led to the conclusion that these materials have a multiphase character on a scale of the order of millimeters, even though they appear homogeneous in x-ray diffraction and electron microscopy. The Seebeck measurements

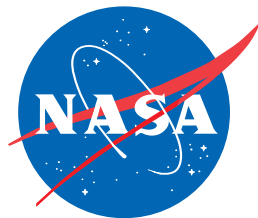
showed significant variations, including both n-type and p-type behavior in the same sample. These variations were found to be consistent with observed variations of ZT . The rapidly quenched samples were found to be less inhomogeneous than were the furnace-cooled ones; hence, rapid quenching was suggested as a basis of research on synthesizing more nearly uniform high- ZT samples.

This work was done by G. Jeffrey Snyder, Nancy Chen, Franck Gascoin, Eckhard Mueller, Gabriele Karpinski, and Christian Stiewe of Caltech for NASA's Jet Propulsion Laboratory. Further information is contained in a TSP (see page 1). NPO-42657

⚙️ Spacecraft Escape Capsule

A report discusses the Gumdrop capsule — a conceptual spacecraft that would enable the crew to escape safely in the event of a major equipment failure at any time from launch through atmospheric re-entry. The scaleable Gumdrop capsule would comprise a command module (CM), a service module (SM), and a crew escape system (CES). The CM would contain a pressurized crew environment that would include avionic, life-support, thermal control, propulsive attitude control, and recovery systems. The SM would provide the primary propulsion and would also supply electrical power, life-support resources, and active thermal control to the CM. The CES would include a solid rocket motor, embedded within the SM, for pushing the CM away from the SM in the event of a critical thermal-protection-system failure or loss of control. The CM and SM would normally remain integrated with each other from launch through recovery, but could be separated using the CES, if necessary, to enable the safe recovery of the crew in the CM. The crew escape motor could be used, alternatively, as a redundant means of de-orbit propulsion for the CM in the event of a major system failure in the SM.

This work was done by Edward A. Robertson, Dingell W. Charles, Ann L. Buskin, Liana M. Rodrigues, Wayne Peterson, Peter Cuthbert, David E. Lee, and Carlos Westhelle of Johnson Space Center. Further information is contained in a TSP (see page 1). MSC-23840



National Aeronautics and
Space Administration